

Hydrodynamics of massless integrable RG flows and a non-equilibrium c-theorem

D. X. Horváth^{a,b}

^a*MTA-BME "Momentum" Statistical Field Theory Research Group,
1111 Budapest, Budafoki út 8, Hungary*

^b*Department of Theoretical Physics,
Budapest University of Technology and Economics,
1111 Budapest, Budafoki út 8, Hungary*

E-mail: esoxluciuslinne@gmail.com

ABSTRACT: We study Euler scale hydrodynamics of massless integrable quantum field theories interpolating between two non-trivial renormalisation group fixed points after inhomogeneous quantum quenches. Using a partitioning protocol with left and right initial thermal states and the recently developed framework of generalised hydrodynamics, we focus on current and density profiles for the energy and momentum as a function of $\xi = x/t$, where both x and t are sent to infinity. Studying the first few members of the A_n and D_n massless flows we carry out a systematic treatment of these series and generalise our results to other unitary massless models.

In our analysis we find that the profiles exhibit extended plateaux and that non-trivial bounds exist for the energy and momentum densities and currents in the non-equilibrium stationary state, i.e. when $\xi = 0$. To quantify the magnitude of currents and densities, dynamical central charges are defined and it is shown that the dynamical central charge for the energy current satisfies a certain monotonicity property. We discuss the connection of the Landauer-Büttiker formalism of transport with our results and show that this picture can account for some of the bounds for the currents and for the monotonicity of the dynamical central charge. These properties are shown to be present not only in massless flows but also in the massive sinh-Gordon model suggesting their general validity and the correctness of the Landauer-Büttiker interpretation of transport in integrable field theories. Our results thus imply the existence of a non-equilibrium c-theorem as well, at least in integrable models. Finally we also study the interesting low energy behaviour of the A_2 model that corresponds to the massless flow from the tricritical to the critical Ising field theory.

Contents

1	Introduction	1
2	Macro-states in integrable models and the GHD	4
2.1	Thermodynamic Bethe Ansatz description for thermal and GGE states	6
2.2	GHD and the partitioning protocol	7
3	Thermodynamics of the A_n and D_n massless flows	9
4	Hydrodynamics of the tricritical to critical Ising flow	12
4.1	Plateaux in the profiles and the dynamical central charges	12
4.2	Low energy behaviour and constant regions in the density/current profiles in the A_2 flow	16
5	Hydrodynamics of the A_n and D_n flows	18
6	The Landauer-Büttiker picture and its implications on transport	22
7	Conclusions	25
A	Low temperature expansion of the GHD equations for the A_2 flow	32
B	Hydrodynamics of the $W_5^3 \rightarrow W_4^3$ massless model	37

1 Introduction

Understanding the out-of-equilibrium dynamics of isolated quantum many-body systems and giving a rigorous foundation of quantum statistical mechanics are one of the most challenging problems in contemporary physics. Thanks to the recent advances in laboratory techniques [1–9] the experimental realisability of closed quantum systems provides a direct insight into quantum statistical physics. As a result of intensive experimental and theoretical investigations, significant progress has been made in the study of non-equilibrium behaviour and recent investigations have led to a series of interesting discoveries. Perhaps the most unusual behaviour is related to integrable quantum systems and the experimental observation of the lack of thermalisation therein [1–3, 10]. Because of their unusual properties, their experimental relevance and analytic tractability, non-equilibrium physics in integrable models continues to attract a lot of attention.

A paradigmatic setting for non-equilibrium dynamics is provided by so-called quantum quenches corresponding to a sudden change in the parameters of a closed quantum system [11, 12]. One of the simplest example is that of a homogeneous system where time

evolution after a quantum quench is expected to lead to relaxation to thermal equilibrium. However, in the case of integrable system thermalisation is absent and the steady state was proposed to be described by the generalised Gibbs ensemble (GGE) [13] which is supported by experimental and theoretical studies [4, 14–27]. Nevertheless, important issues such as a theoretical description of the eventual time evolution, as well as the complete set of relevant conserved quantities necessary for the construction of the steady state ensemble are still open in general.

Inhomogeneous quenches, in general, pose a more difficult problem than homogeneous ones with fewer exact or approximate results [28–36]. One promising approach exploits hydrodynamical description assuming the separation of spatial and temporal scales and a local (GGE) equilibrium, and is supported both by numerical simulations and experimental observations [37–41]. Based on the previously mentioned assumptions and on the functional completeness of conserved quantities a hydrodynamical description of integrable systems named Generalised Hydrodynamics (GHD) was developed in [42–44]. In its simplest form the GHD describes the exact average densities and currents associated with conserved quantities at the Euler scale, that is when $x, t \rightarrow \infty$ such that their ratio is fixed. The appearance of non-trivial physics in this limit is in accordance with the ballistic spreading of quasi-particles in integrable models and in many relevant situations the GHD predictions become valid after a relatively short transient time interval [37–40]. The GHD approach has been applied to various systems including spin chains and the Hubbard model [43, 45–52], classical gases and fields [53–56] and quantum gases and fields [38, 42, 57, 58]. Interesting view points on the GHD approach are given in [59–61]. Besides the Euler scale description of current and density averages in various integrable models important new directions are understanding the fluctuations of the hydrodynamic quantities [62, 63] and incorporating diffusive effects which requires going beyond the Euler scale in the GHD description [64–66].

The aim of the present paper is to introduce a renormalisation group perspective and connect the GHD description of the non-equilibrium dynamics of integrable quantum field theories to their formulation as relevant perturbations of conformal field theories (CFT) [67]. In the works [68–74] a rather extensive description of transport properties of out-of-equilibrium CFTs was given. The non-equilibrium setting was provided by the (bi-) partitioning protocol, in which two semi-infinite and independent systems described by the same Hamiltonian are prepared in different initial states, typically in two thermal states with different temperatures. The left and right semi-infinite systems are joined together at a given time and the subsequent time-evolution is governed by the full and homogeneous Hamiltonian acting on the whole space. In the resulting dynamics for CFTs, two shock waves originating from the boundary point move with the speed of light to the left and right directions and in the expanding region between the waves a non-equilibrium steady-state (NESS) emerges. The NESS is obtained in the limit $t \rightarrow \infty$ for finite x and therefore corresponds to $\xi = 0$, supporting non-trivial flows of currents while the asymptotic left ($\xi < 0$) and right ($\xi > 0$) regions act as effective heat reservoirs. In [69–73] the properties of the NESS, current and density averages, fluctuation spectrums for large deviations and correlation functions in the NESS were studied. In particular for CFTs the average energy density q_e and energy current j_e are given by

$$\begin{aligned} q_e &= \frac{c\pi}{12} (T_l^2 + T_r^2) \\ j_e &= \frac{c\pi}{12} (T_l^2 - T_r^2) , \end{aligned} \tag{1.1}$$

where T_l and T_r are the initial left and right temperatures and c is the central charge of the CFT. Due to relativistic invariance j_e equals the momentum density q_p and due to conformal invariance q_e equals the momentum current j_p (and also the pressure).

These results are also valid for systems at or sufficiently close to their critical points but a certain neighbourhood of the critical point or more precisely a certain type of irrelevant perturbation of the fixed point CFT was also studied in [72]. In general, the vicinity of critical points are described by (relevant) perturbations of the critical theory resulting in either a massive quantum field theory (QFT) or a crossover to an infrared (long-distance) fixed point. The high energy behaviour and consequently the high temperature transport properties of such a system are captured by the fixed point CFT, but the intermediate and low energy physics is generally not known. If the perturbed CFT is integrable, which is quite often the case of interest, the GHD approach can be used to explore the transport properties at all scales of the field theory.

Some relevant perturbations of CFTs give rise to massless QFTs, which host massless excitations. For these interpolating renormalisation group flows describing crossover behaviour the high- and low-energy properties are dictated by CFTs. The massless models are not conformal invariant theories and transition from the ultra-violet (UV) CFT to the infra-red (IR) occurs at the characteristic energy scale M called the crossover scale.

Integrable massless flows have a long history and many of them have a detailed description based on the standard techniques of integrability such as S-matrix bootstrap, thermodynamic Bethe Ansatz (TBA) and form factor bootstrap. In this paper we primarily focus on the so-called A_n and D_n massless flows. The A_n models interpolate between multi-critical Ising field theories [75–77] corresponding to the conformal minimal models $\mathcal{M}_{n+2} \rightarrow \mathcal{M}_{n+1}$ whereas the D_n flows describe the crossover between the \mathbb{Z}_n parafermion model and \mathcal{M}_{n+1} [78]. The S-matrices of these models and the corresponding TBA equations are well-known [75–79] together with certain form factors [80–82] and correlation functions [80] for the A_2 case, and it is worth noting the interesting connection of these flows to roaming trajectories and staircase models [83–87].

As these theories interpolate between a UV and an IR conformal field theory, it is natural to investigate the crossover in terms of transport behaviour. This is what the present work aims to accomplish by applying the GHD approach to the partitioning protocol and focusing on the interpolation between the behaviour of the fixed point CFTs describing the endpoints of the RG flow.

The paper is organised as follows. In section 2 the description of homogeneous and inhomogeneous macro-states in terms of the TBA type equations is discussed for integrable models and the main ideas of the GHD approach are summarised. In section 3 some elements of the thermodynamics of the A_n and D_n flows are discussed that are useful to understand the inhomogeneous problem. Section 4 is devoted to hydrodynamics of the A_2

model. Besides reviewing its interesting low temperature limit, we identify features that are later shown to be generally present in massless models and introduce the notion of dynamical central charges. In section 5 the discussion is generalised to higher members of the A_n and D_n hierarchy of massless flows. In section 6 we establish a connection with the Landauer-Büttiker (LB) theory of transport and discuss its implications for the dynamical central charges in RG flows. In this section the transport of massive sinh-Gordon integrable QFT is also studied and compared to the LB results, and we show that all the results suggest an out-of-equilibrium version of the c-theorem [88, 89], at least for relativistic integrable QFTs. Finally we conclude in section 7. Some details are relegated to appendices: in appendix A, the low-temperature expansion of the TBA and GHD equations are performed for the A_2 model, while appendix B discusses the hydrodynamics of the $W_5^3 \rightarrow W_4^3$ massless flow.

2 Macro-states in integrable models and the GHD

In this section we briefly review how macro-states such as homogeneous thermal or inhomogeneous locally quasi-stationary states (LQSS) can be characterised in integrable models and discuss the main ideas behind the GHD approach. For most integrable models, the spectrum of energy levels can be described in terms of stable quasi-particles excitations. Averages of local operators in macro states can be constructed by representing the corresponding density matrices in terms of continuous densities associated with the distribution of these stable quasi-particles. In particular the so-called root density $\rho(\vartheta)$ gives the number of quasiparticles in the range $[\vartheta, \vartheta + \Delta\vartheta]$, which is $L\rho(\vartheta)\Delta\vartheta$, if L is the system size and the rapidity ϑ parametrizes the energy and momentum of the quasi-particles. In the case of additional quantum numbers or different species of quasi-particles, multiple root densities labeled by the appropriate quantum numbers are required.

Similarly to the root densities one can introduce the hole densities $\rho_h(\vartheta)$ as well, which are associated with unoccupied one-particle energy levels. The root and hole densities are not independent quantities due to the interaction between the quasiparticles. Extending our description to models with n quasiparticle species and with diagonal scattering, the root and hole densities ρ_j and $\rho_{j,h}$ corresponding to the different species satisfy the Bethe Ansatz equations

$$\rho_j(\vartheta) + \rho_{j,h}(\vartheta) = \frac{1}{2\pi} p'_j(\vartheta) + \sum_{k=1}^n (\varphi_{jk} \star \rho_k)(\vartheta). \quad (2.1)$$

In (2.1), $p'_j(\vartheta)$ denotes the derivative of the one-particle momentum of the j th species with respect to the rapidity ϑ , φ_{jk} is specified by the two-particle scattering matrix S_{jk} as

$$\varphi_{jk}(\vartheta) = -i \frac{d}{d\vartheta} \ln(-S_{jk}(\vartheta)), \quad (2.2)$$

and the symbol \star denotes convolution:

$$(f \star g)(\vartheta) = \int_{-\infty}^{\infty} \frac{d\vartheta'}{2\pi} f(\vartheta - \vartheta') g(\vartheta'). \quad (2.3)$$

It is convenient to introduce the filling functions $n_j(\vartheta)$ and the pseudo-energies $\varepsilon_j(\vartheta)$ via

$$n_j(\vartheta) = \frac{\rho_j(\vartheta)}{\rho_j(\vartheta) + \rho_{j,h}(\vartheta)} = \frac{1}{e^{\varepsilon_j(\vartheta)} + 1}, \quad (2.4)$$

with $j = 1, \dots, n$ and also the dressing operation for a set of functions $f_j(\vartheta)$ with $j = 1, \dots, n$ by the solution of the integral equation

$$f_j^{\text{dr}}(\vartheta) = f_j(\vartheta) + \sum_{k=1}^n (\varphi_{jk} \star n_k f_k^{\text{dr}})(\vartheta). \quad (2.5)$$

Given the root and hole densities or the filling functions, the densities of various extensive quantities can be easily calculated in the macro-state. For conserved charges Q_i with one-particle eigenvalue $h_j^{(i)}(\vartheta)$ with respect to the j th particle species, that is

$$Q_i |\vartheta\rangle_j = h_j^{(i)}(\vartheta) |\vartheta\rangle_j,$$

the corresponding density q_i can be expressed equivalently as

$$\begin{aligned} q_i &= \sum_{j=1}^n \int_{-\infty}^{\infty} \frac{d\vartheta}{2\pi} h_j^{(i)}(\vartheta) \rho_j(\vartheta), \\ &= \sum_{j=1}^n \int_{-\infty}^{\infty} \frac{d\vartheta}{2\pi} (p_j'(\vartheta))^{\text{dr}} n_j(\vartheta) h_j^{(i)}(\vartheta) \\ &= \sum_{j=1}^n \int_{-\infty}^{\infty} \frac{d\vartheta}{2\pi} p_j'(\vartheta) n_j(\vartheta) \left(h_j^{(i)}(\vartheta) \right)^{\text{dr}}. \end{aligned} \quad (2.6)$$

Similarly to the quantum mechanical operator \mathbf{q}_i , which is the density of the charge Q_i , the average of the corresponding current \mathbf{j}_i in the macro-state can be expressed in terms of the filling functions or root densities. Before quoting the expressions we first introduce the effective velocity $v_j^{\text{eff}}(\vartheta)$ defined as

$$v_j^{\text{eff}}(\vartheta) = \frac{\left(e_j'(\vartheta) \right)^{\text{dr}}}{\left(p_j'(\vartheta) \right)^{\text{dr}}}. \quad (2.7)$$

While the velocity of a single particle can be defined as

$$\frac{e_j'(\vartheta)}{p_j'(\vartheta)},$$

the dressing in (2.7) accounts for the effect of other quasi-particles in the macro-state specified by the root densities. Due to scattering processes, the single-particle velocity is modified according to (2.7).

With the effective velocity, the averages j_i of \mathbf{j}_i can be written as

$$\begin{aligned}
j_i &= \sum_{j=1}^n \int_{-\infty}^{\infty} \frac{d\vartheta}{2\pi} v_j^{\text{eff}}(\vartheta) h_j^{(i)}(\vartheta) \rho_j(\vartheta) \\
&= \sum_{j=1}^n \int_{-\infty}^{\infty} \frac{d\vartheta}{2\pi} (e'_j(\vartheta))^{\text{dr}} n_j(\vartheta) h_j^{(i)}(\vartheta) \\
&= \sum_{j=1}^n \int_{-\infty}^{\infty} \frac{d\vartheta}{2\pi} e'_j(\vartheta) n_j(\vartheta) \left(h_j^{(i)}(\vartheta) \right)^{\text{dr}} .
\end{aligned} \tag{2.8}$$

The expressions were first proposed in [42] and later verified for relativistic QFT in [90]. These equations are in accordance with the ballistic transport of conserved quantities in integrable models.

Finally, we mention that the entropy density s of the macro-state can be written as

$$s = \sum_{j=1}^n \int_{-\infty}^{\infty} d\vartheta [\rho_{j,t}(\vartheta) \ln \rho_{j,t}(\vartheta) - \rho_j(\vartheta) \ln \rho_j(\vartheta) - \rho_{j,h}(\vartheta) \ln \rho_{j,h}(\vartheta)] . \tag{2.9}$$

2.1 Thermodynamic Bethe Ansatz description for thermal and GGE states

The root densities or the filling functions of homogeneous and global thermal and GGE states can be obtained by solving the Thermodynamic Bethe Ansatz (TBA) equations

$$\varepsilon_j(\vartheta) = w_j(\vartheta) - \left(\sum_{k=1}^n \varphi_{jk} \star \ln(1 + e^{-\varepsilon_k}) \right) (\vartheta) , \tag{2.10}$$

where the driving term reads

$$w_j(\vartheta) = \sum_{i=1}^{\infty} \beta_i h_j^{(i)}(\vartheta) , \tag{2.11}$$

if the state to describe is a GGE state with density matrix

$$\rho_{GGE} = \frac{1}{Z} e^{-\sum \beta_i Q_i} , \tag{2.12}$$

with generalised chemical potentials β_i associated with each conserved charge. For the particular case of thermal states, w_j is merely

$$w_j(\vartheta) = \frac{1}{T} e_j(\vartheta) , \tag{2.13}$$

where T is the temperature. The corresponding free-energy density or generalised free-energy density $f = F/L$ with $F = \sum \beta_i \langle Q_i \rangle - S$ can be calculated by

$$f = \sum_{k=1}^n \int_{-\infty}^{\infty} d\vartheta p'_k(\vartheta) \ln(1 + e^{-\varepsilon_k(\vartheta)}) . \tag{2.14}$$

From the thermal free energy density the effective central charge

$$\tilde{c}(T) = \frac{1}{T} \frac{3}{\pi^2} \sum_{k=1}^n \int_{-\infty}^{\infty} d\vartheta p'_k(\vartheta) \ln \left(1 + e^{-\varepsilon_k(\vartheta)} \right) \quad (2.15)$$

can be obtained, which plays an important role in our subsequent considerations. Due to the c-theorem [89], $\tilde{c}(T)$ increases monotonously with the temperature¹ and signals the amount of the effective degrees of freedom in the field theory. In the $T \rightarrow \infty$ limit its value is determined by the UV limiting conformal field theory, in particular

$$\lim_{T \rightarrow \infty} \tilde{c}(T) = c_{UV} , \quad (2.16)$$

where c_{UV} is the central charge of the UV conformal field theory if it is unitary. In the $T \rightarrow 0$ limit, \tilde{c} is zero in massive models but equals the central charge of the IR conformal field theory for massless flows

$$\lim_{T \rightarrow 0} \tilde{c}(T) = \begin{cases} 0 & \text{massive case} \\ c_{IR} & \text{massless case} . \end{cases} \quad (2.17)$$

2.2 GHD and the partitioning protocol

The main purpose of our paper is to study transport properties of massless integrable models in inhomogeneous initial states. To treat inhomogeneous situations, it is convenient to apply a hydrodynamic approach relying on the separation of space and time scales and on the assumption of local equilibration. The large-scale behaviour of inhomogeneous systems can be described by a space-time dependent GGE

$$\rho_{GGE} = \frac{1}{Z} e^{-\sum \int dx \beta_i(x,t) \mathbf{q}_i(x)} , \quad (2.18)$$

and consequently the large-scale expectation values of local operators can be obtained as

$$\langle \mathcal{O}(x,t) \rangle = \langle \mathcal{O} \rangle_{x,t} , \quad (2.19)$$

where

$$\langle \mathcal{O} \rangle_{x,t} = \frac{1}{Z} \text{Tr} \mathcal{O}(0,0) e^{-\sum \beta_i(x,t) Q_i} . \quad (2.20)$$

Similarly to the homogeneous case, (x,t) -dependent root densities $\rho_j(\vartheta, x, t)$ and filling functions $n_j(\vartheta, x, t)$ can be introduced to describe the LQSS. Exploiting eqs. (2.19) and (2.20), the continuity equation of the conserved quantities $\partial_t \mathbf{q}_i + \partial_x \mathbf{j}_i = 0$ transforms into

$$\partial_t q_i(x,t) + \partial_x j_i(x,t) = 0 , \quad (2.21)$$

where

¹In its most commonly formulated version, the effective central charge \tilde{c} entering the c-theorem is a function of the distance R instead of the temperature T .

$$\begin{aligned} q_i(x, t) &= \langle \mathbf{q}_i \rangle_{x, t} \\ j_i(x, t) &= \langle \mathbf{j}_i \rangle_{x, t} . \end{aligned} \quad (2.22)$$

In integrable models, assuming a sufficient functional completeness of the conserved charges, the continuity equation for the LQSS averages (2.21) can be recast in many different forms including the space-time dependent root densities or filling functions. For our purposes, the most direct rewriting reads [42]

$$\partial_t n_j(\vartheta, x, t) - v_j^{\text{eff}}[\vartheta, \{n_j(\vartheta, x, t)\}] \partial_x n_j(\vartheta, x, t) = 0, \quad (2.23)$$

where v_j^{eff} is defined by eq. (2.7) and the argument in the bracket stresses that v_j^{eff} is a complicated functional of the set of filling functions n_j which now depend on space and time besides the rapidity. The equation (2.23) is in complete agreement with the ballistic spreading of quasi-particles in integrable models. The effect of the interactions is incorporated in the effective velocity of the quasi-particles. For the case of the partitioning protocol corresponding to an initial density matrix

$$\rho_0 \propto \rho_l \otimes \rho_r, \quad (2.24)$$

which is different on the left and right halves of the system, eq. (2.23) can be solved in a particularly simple way. For the particular case of thermal states considered in this paper, the initial density matrix reads

$$\rho_0 = \frac{1}{Z} e^{-\beta_l H_l} \otimes e^{-\beta_r H_r}, \quad (2.25)$$

where the Hamiltonians H_l and H_r act in the left and right half-spaces. The two halves are joined together at time $t = 0$ and subsequent time evolution is governed by the homogeneous Hamiltonian acting on the whole space. To be precise, some boundary conditions have to be prescribed for H_r and H_l at the position $x = 0$ before $t = 0$; nevertheless, it is expected that their effect becomes negligible at the Euler scale. Consequently, the initial condition for $n_j(\vartheta, x, 0)$ can be written as

$$n_j(\vartheta, x, 0) = \Theta_H(x) n_j^{(r)}(\vartheta) + \Theta_H(-x) n_j^{(l)}(\vartheta), \quad (2.26)$$

where Θ_H is the Heaviside function and $n_j^{(r)}$ and $n_j^{(l)}$ are the filling functions corresponding to the right and left density matrices describing homogeneous thermal (or GGE in general) states with temperatures T_r and T_l . To obtain a solution of (2.23) with an initial condition for n_j compatible with (2.26) it is exploited that both the differential equations (2.23) and the initial condition (2.26) are invariant under the reparametrisation $x, t \rightarrow \lambda x, \lambda t$. As a consequence the solution of (2.23) depends only on the ratio x/t which we denote by ξ and call a ray. The corresponding ray-dependent continuity equations read

$$-\xi \partial_\xi q_i(\xi) + \partial_\xi j_i(\xi) = 0, \quad (2.27)$$

and

$$(\xi - v_j^{\text{eff}}[\{n_j(\vartheta, \xi)\}]) \partial_\xi n_j(\vartheta, \xi) = 0, \quad (2.28)$$

and the implicit solution of the latter is given by

$$n_j(\vartheta, \xi) = \Theta_H(v_j^{\text{eff}}(\vartheta, \xi) - \xi) n_j^{(l)}(\vartheta, \xi) + \Theta_H(\xi - v_j^{\text{eff}}(\vartheta, \xi)) n_j^{(r)}(\vartheta, \xi). \quad (2.29)$$

Its interpretation in terms of the ballistic spreading of quasi-particles is natural; quasi-particles that contribute at the ray ξ come from the left if their effective velocity is larger than ξ and they come from the right side if their effective velocity is slower than ξ ; the effective velocity depends on all the other particles due to the elastic scattering between them. The self-consistent numerical solution of the above equation is usually straightforward to obtain by iteration. In particular when $v_j^{\text{eff}}(\vartheta, \xi)$ is a monotonously increasing function of ϑ for all ξ , the solution can be rewritten as

$$n_j(\vartheta, \xi) = \Theta_H(\vartheta - \vartheta_j) n_j^{(l)}(\vartheta, \xi) + \Theta_H(\vartheta_j - \vartheta) n_j^{(r)}(\vartheta, \xi), \quad (2.30)$$

where ϑ_j is determined by the implicit equations

$$v_j^{\text{eff}}(\vartheta_j) = \xi \quad (2.31)$$

for all j and v_j^{eff} , which is a functional of all $n_j(\vartheta, \xi)$, is determined by (2.7). As discussed in section 3, the effective velocities of magnonic particles can be monotonously decreasing or non-monotonous functions of the rapidity too. In such a case (2.30) may include more terms, and more than a single ϑ_j is necessary to use to describe the jumps in the filling functions. The values of the $\vartheta_j^{(m)}$ parameters are still to be determined by (2.7) for all m in a self-consistent manner.

In massless models the effective velocities of the quasi-particles (either the later introduced right- and left-moving particles or the magnons are regarded) usually do not cover the full $[-1, 1]$ interval but only its subset $[v_j^{\text{min}}, v_j^{\text{max}}]$. In such a case the solution of (2.28) for a ray $\xi \in [-1, v_j^{\text{min}}]$ is $n_j^{(l)}(\vartheta)$ since there are only faster than ξ particles, which must come from the left and similarly for a ray $\xi \in [v_j^{\text{max}}, 1]$ it is $n_j^{(r)}(\vartheta)$ (where $n_j^{(l)}(\vartheta)$ and $n_j^{(r)}(\vartheta)$ are the filling functions of the homogeneous left/right thermal states or GGE). This situation is similar to what was discussed in [91], which focused on the transport of non-linear Luttinger liquids.

Once $n_j(\vartheta, \xi)$ are determined, the ray-dependent averages of the densities and currents of conserved charges can be straightforwardly calculated using (2.5), (2.6) and (2.8).

3 Thermodynamics of the A_n and D_n massless flows

In this section we review on the finite temperature description of integrable massless flows using the TBA. The finite temperature filling functions are essential inputs for the hydrodynamics of the partitioning protocol, moreover many peculiar features of the emerging hydrodynamics can be understood by analysing the homogeneous, finite temperature case.

The TBA equations for massless flows associated with the A_n and D_n series can be written [79] as

$$\varepsilon_j(\vartheta) = w_j(\vartheta) - \left(\sum_{k=1}^n \varphi \star \ln(1 + e^{-\varepsilon_k}) G_{jk} \right)(\vartheta), \quad (3.1)$$

where

$$\varphi(\vartheta) = \frac{1}{\cosh \vartheta}, \quad (3.2)$$

G_{jk} is the adjacency matrix of the A_n and D_n Dynkin diagrams (c.f. figure 1) and the source terms read

$$\begin{aligned} w_j(\vartheta) &= \frac{M}{2T} \left(e^{\vartheta} \delta_{j,1} + e^{-\vartheta} \delta_{j,n} \right) \text{ for } A_n, n \geq 2 \\ w_j(\vartheta) &= \frac{M}{2T} \left(e^{\vartheta} \delta_{j,n-1} + e^{-\vartheta} \delta_{j,n} \right) \text{ for } D_n, n \geq 3. \end{aligned} \quad (3.3)$$

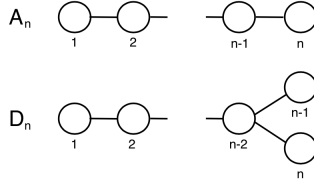


Figure 1: Dynkin diagrams of the A_n and D_n Lie algebras

The nodes in the diagrams correspond to different particle species. The scattering between these species is non-trivial only for the neighbouring nodes. According to eq. (3.3) only two nodes in the Dynkin diagrams couple to non-vanishing driving terms. The source terms $\frac{M}{2T}e^{\pm\vartheta}$ correspond to right- and left-moving i.e. (RM) and (LM) particles, whose one-particle energy and momentum are $\frac{M}{2}e^{\pm\vartheta}$ and $\pm\frac{M}{2}e^{\pm\vartheta}$ respectively. The energy scale M is the crossover scale, which separates the low and high energy regimes dominated by the UV and IR limiting CFTs. The other nodes in the Dynkin diagrams correspond to magnons, which describe internal degrees of freedom of the quasi-particle excitations. It is important to note that although the magnonic excitations themselves may be regarded as quasi-particles, they have zero one-particle eigenvalues with respect to the conserved charge operators, hence quantities such as the energy or momentum are carried by only the RM and LM species.

The eventual identification of the models described by the TBA equations is a non-trivial task. The A_n flows interpolate between multi-critical Ising field theories [75–77] according to $\mathcal{M}_{n+2} \rightarrow \mathcal{M}_{n+1}$ with

$$\begin{aligned} c_{UV} &= 1 - \frac{6}{(n+2)(n+3)} \\ c_{IR} &= 1 - \frac{6}{(n+1)(n+2)}. \end{aligned} \quad (3.4)$$

These integrable RG trajectories are the $\phi_{1,3}$ perturbations with scaling dimension $\Delta = 1 - \frac{2}{n+3}$ of the UV conformal theory \mathcal{M}_{n+2} [75–77]. For the A_n massless models, both c_{UV} and c_{IR} tends to 1 as $n \rightarrow \infty$ and the difference between the UV and IR central charges vanishes in this limit.

The D_n flows describe the crossover between the \mathbb{Z}_n parafermion model and \mathcal{M}_{n+1} [78] with

$$\begin{aligned} c_{UV} &= \frac{2(n-1)}{n+2} \\ c_{IR} &= 1 - \frac{6}{(n+1)(n+2)} \end{aligned} \quad (3.5)$$

and are obtained by adding the perturbing operator $\psi_1(z)\bar{\psi}_1(\bar{z}) + \psi_1^\dagger(z)\bar{\psi}_1^\dagger(\bar{z})$ with dimension $1 - \frac{1}{n}$ [79] to the UV limiting CFT. Here in the $n \rightarrow \infty$ limit $c_{UV} = 2 \neq c_{IR} = 1$.

For thermal states the filling function of the RM and LM particles are of a very peculiar form in all massless integrable models: they are kinks related by $n_{RM}(\vartheta) = n_{LM}(-\vartheta)$. Focusing on n_{RM} for $\vartheta \rightarrow -\infty$ its value is a constant and for $\vartheta \rightarrow \infty$ it goes to zero as $\exp(-M(\exp \vartheta)/(2T))$. This behaviour is illustrated on figure 2 for the case of the D_4 massless model.

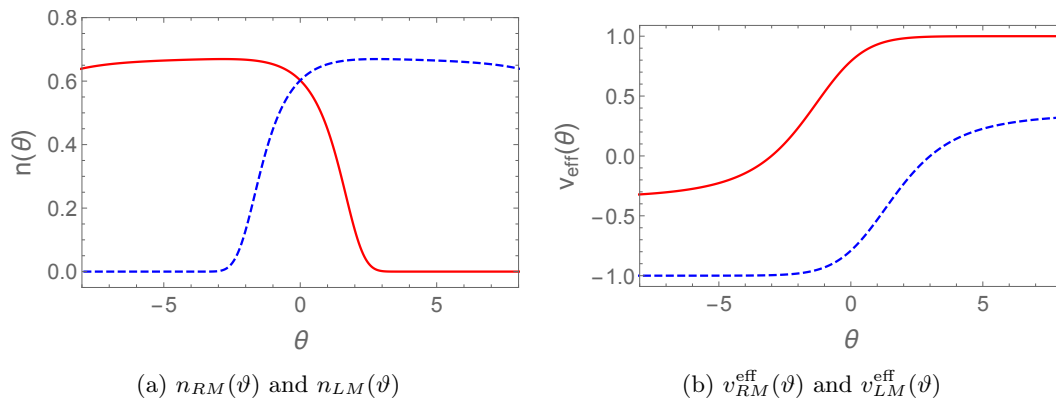


Figure 2: (a) Filling function of right-moving (red continuous curve) and left-moving particles (blue dashed curve) and (b) the effective velocities of the right-moving (red continuous curve) and left-moving (blue dashed curve) particles in the D_4 flow in a thermal state with $T/M = 1.4$.

Although the bare velocities of the RM and LM particles are ± 1 in units of the speed of light, in highly-excited states such as thermal states the effective velocities are different from ± 1 due to interactions which results in non-trivial kinetics in the GHD setting. The TBA description of the D_4 flow also includes two magnonic particles, whose effective velocities can even be non-monotonous functions of the rapidity as demonstrated by figure 3.

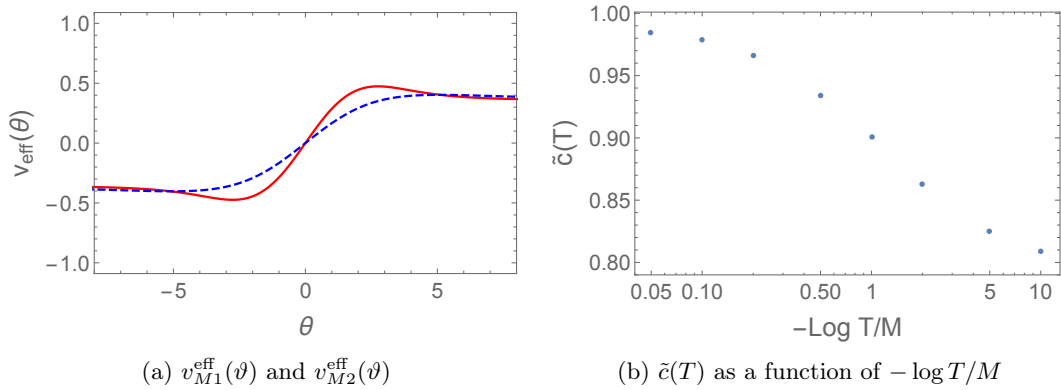


Figure 3: (a) the effective velocities of the first (red continuous curve) and second (blue dashed curve) magnons in the D_4 flow in a thermal state with $T/M = 1.4$. The first and the second magnons correspond to the first and second nodes in the D_4 Dynkin diagram. (b) The c -theorem for the D_4 massless model. The \tilde{c} function interpolates between the UV and IR central charges whose values are 1 and 0.8.

Finally, to conclude this section subfigure (b) in figure 3 shows the c -function as a function $-\log T/M$ for the D_4 massless model.

4 Hydrodynamics of the tricritical to critical Ising flow

In this section we focus on the Euler scale hydrodynamics of the A_2 flow after a bipartite quench. The A_2 model, whose UV and IR limiting theories are the tricritical and critical Ising CFTs [75, 76], is the simplest massless flow with a RM and LM particle in the TBA equations. By solving first the corresponding TBA equations (3.1) with (3.3) for the left and right filling functions and then the final form of the GHD equations (2.30) and (2.31), the ray-dependent density and current profiles are easy to obtain from eqs. (2.6) and (2.8). We start our analysis by first discussing some peculiar features of these profiles such as the existence of extended plateaux and the bounds on the currents and densities which turn out to be quite generic for all massless models studied in this work.

4.1 Plateaux in the profiles and the dynamical central charges

Figure 4 shows the ray-dependent energy and momentum densities and currents and one peculiar feature of these quantities are the extended plateaux in the currents and densities. As discussed in the introduction, the Euler scale behaviour of these quantities in CFTs are described by exactly flat plateaux and discontinuous jumps at $\xi = \pm 1$. Since both at low and high energies, i.e. low and high temperatures the limiting theories of massless models are CFTs, one should not be surprised about the emergence of similar plateaux in the massless flows. It is slightly more interesting that the plateaux still exist outside the conformal regimes where the left and right temperatures are close to the inverse of the crossover scale M^{-1} , corresponding to the massless flow being far away from the conformal limits.

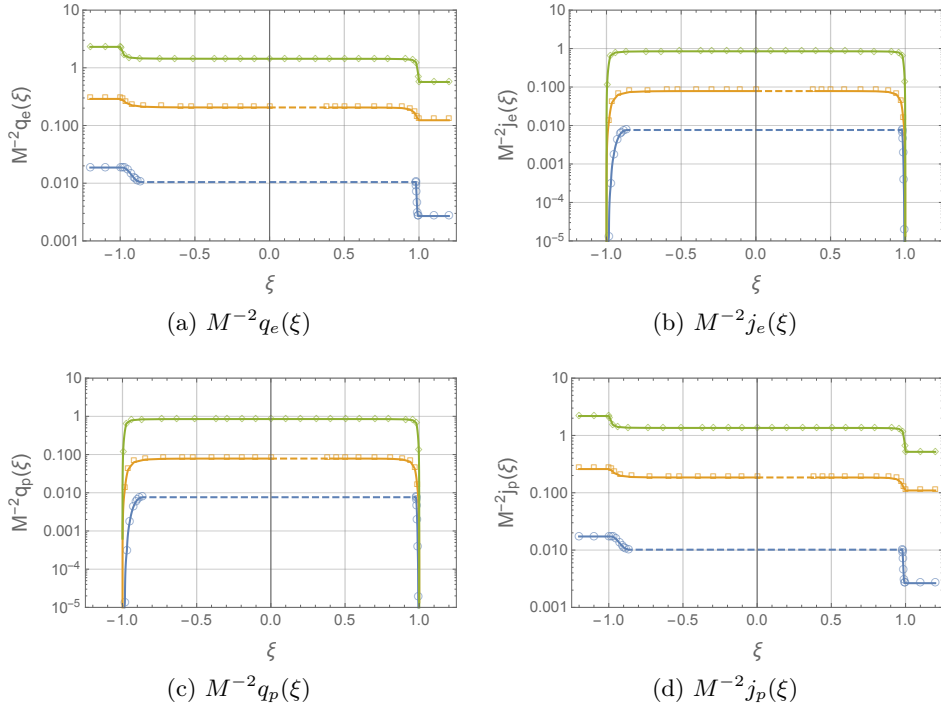


Figure 4: Ray-dependent (a) energy density q_e , (b) energy current j_e , (c) momentum density q_p and (d) momentum current j_p in the A_2 tricritical to critical Ising flow after bipartite quenches at the Euler scale. The green curve with diamonds corresponds to left and right initial temperatures $T_l = 2.5M$ and $T_r = 1.25M$, the orange curve with squares to $T_l = 0.9M$ and $T_r = 0.6M$ and the blue curve with circles to $T_l = 0.25M$ and $T_r = 0.1M$. The discrete points in the plots indicated by the plotmarkers are obtained by the numerical solution of GHD equations, the continuous curves are first order interpolations. The dashed part of the curves indicates the region of constant densities and currents. Due to relativistic invariance, $j_e = q_p$.

The existence of the plateaux in this regime can be understood from the TBA equations using that in thermal states the filling functions n_{RM} and n_{LM} are kinks. Whereas these kinks possess some structure, they can be roughly regarded as Heaviside theta functions. The transition from a non-zero value to zero takes place at a temperature dependent rapidity, which we can denote as $\vartheta_{RM/LM}^{(r)/(l)}$ depending on the species and its leading order temperature dependence is logarithmic (c.f. eqs. (2.4), (3.1) and (3.3)). In the bipartite quench protocol the left and right filling functions are joined together according to (2.30) and the transition from the right filling function to the left in $n_{RM}(\vartheta, \xi) = n_{RM}(\vartheta, \vartheta_{RM})$ and $n_{LM}(\vartheta, \xi) = n_{LM}(\vartheta, \vartheta_{LM})$ takes place at a rapidity ϑ_{RM} and ϑ_{LM} respectively. When the rapidities ϑ_{RM} and ϑ_{LM} sweep through the real interval and the filling functions are approximated by theta functions, $n_{RM}(\vartheta, \vartheta_{RM})$ and $n_{LM}(\vartheta, \vartheta_{LM})$ are either the left or right filling functions apart from the case when $\vartheta_{RM} \in [\vartheta_{RM}^{(r)}, \vartheta_{RM}^{(l)}]$ and $\vartheta_{LM} \in [\vartheta_{LM}^{(l)}, \vartheta_{LM}^{(r)}]$. For sufficiently high temperature with a not too large difference between the left and right values these rapidity intervals are very short. Although the ray ξ is a generally function of both ϑ_{RM} and ϑ_{LM} , the regions of ξ where the right-left transition occurs in

$n_{RM}(\vartheta, \xi)$ and $n_{LM}(\vartheta, \xi)$ remain narrow. These regions correspond to the sharp transitions in the density and current profiles, whereas for the the left, middle and right plateaux $n_{RM}(\vartheta, \xi) = n_{RM}^{(l)}(\vartheta)$, $n_{LM}(\vartheta, \xi) = n_{LM}^{(l)}(\vartheta)$; $n_{RM}(\vartheta, \xi) = n_{RM}^{(l)}(\vartheta)$, $n_{LM}(\vartheta, \xi) = n_{LM}^{(r)}(\vartheta)$ and $n_{RM}(\vartheta, \xi) = n_{RM}^{(r)}(\vartheta)$, $n_{LM}(\vartheta, \xi) = n_{LM}^{(r)}(\vartheta)$ respectively. Of course, the left and right filling functions are not exact Heaviside theta functions and hence the middle plateaux are not exactly flat.

Our argument seems to be invalid when the difference between the left and right temperatures is large. In such a case, however, the high energy particles almost exclusively originate from the left side and hence the UV limiting CFT dominates the dynamics as supported by table 1 discussed shortly. In summary, irrespectively of the magnitude of the left and right temperatures, the plateaux in the energy and momentum density and current profiles are a generic feature the Euler scale hydrodynamics of the A_2 massless flow. As demonstrated in the next section, the extended plateaux also occur in other massless integrable theories.

T_l/M	T_r/M	$\tilde{c}(T_l)$	$\tilde{c}(T_r)$	$\tilde{c}_{j_e}(T_l, T_r)$	$\tilde{c}_{q_e}(T_l, T_r)$	$\tilde{c}_{j_p}(T_l, T_r)$	$\tilde{c}_{j_e}^{lb}(T_l, T_r)$
0.25	0.1	0.527539	0.505141	0.555744	0.551405	0.535171	0.531832
0.9	0.1	0.610694	0.505141	0.642663	0.645557	0.633447	0.634259
0.9	0.6	0.610694	0.581244	0.666046	0.670596	0.603226	0.612022
0.95	0.9	0.614468	0.610694	0.675198	0.682408	0.612715	0.64752
1.4	0.9	0.639252	0.610694	0.682109	0.691041	0.631924	0.659371
2.5	1.25	0.666775	0.632483	0.691766	0.700926	0.66099	0.678208
6	0.2	0.68853	0.519057	0.695114	0.698746	0.69212	0.68872
6	5	0.68853	0.685515	0.698716	0.70355	0.68731	0.695382
6.5	6	0.689664	0.68853	0.69897	0.703259	0.689146	0.696195
9	6	0.693292	0.68853	0.699239	0.702619	0.691869	0.697102
9	8.5	0.693292	0.692755	0.69942	0.702409	0.693041	0.697723

Table 1: The effective central charges for (left and right) thermal states and the dynamical central charges for the partitioning protocol for various left and right temperatures in the A_2 massless flow, where $c_{UV} = 0.7$ and $c_{IR} = 0.5$.

To discuss a second characteristic feature, we first define a dynamical central charge inspired by (1.1) by writing

$$j_e(0) = q_p(0) = \frac{\tilde{c}_{j_e}(T_l, T_r)}{12\pi} (T_l^2 - T_r^2) . \quad (4.1)$$

The dynamical central charge \tilde{c}_{j_e} (together with its counterparts for the cumulants of the transferred energy) was already defined and used in [92] for non-equilibrium situations. Calculating the energy current (or momentum density) at the ray $\xi = 0$, \tilde{c}_{j_e} can easily be obtained knowing the left and right temperatures. Whereas in CFTs the energy current $j_e(\xi)$ is constant if $\xi \in (-1, 1)$, for the massless flows $j_e(\xi)$ usually exhibits a non-trivial ξ -dependence, therefore we must specify at which ray ξ j_e is to take in order to define \tilde{c}_{j_e} .

It seems natural to choose ξ at which j_e is maximal, which occurs at $\xi = 0$ as a consequence of the continuity equation (2.27). Moreover, taking the limit $t \rightarrow \infty$ at any fixed position x gives the NESS, which also corresponds to $\xi = 0$.

In table 1 the values of \tilde{c}_{j_e} are collected for various left and right temperatures together with the effective central charges for the left and right thermal states. Based on the data we propose the following conjecture for the dynamical central charge in bipartite quenches with left and right initial thermal states:

$$c_{IR} \leq \tilde{c}(\max(T_r, T_l)) \leq \tilde{c}_{j_e}(T_l, T_r) \leq c_{UV}. \quad (4.2)$$

This is an interesting property of the dynamical central charge which (4.2) also implies upper and lower bounds on the maximum of the ray-dependent energy current or equivalently the current in the NESS, and an upper bound for the energy current at any ray. In [93] a lower bound for the steady-state energy current was given, which reads in our case

$$j_e(0) \geq \frac{\langle \mathbf{j}_p \rangle_{\beta_l} - \langle \mathbf{j}_p \rangle_{\beta_r}}{2}, \quad (4.3)$$

where the averages of the momentum current are taken in the left and right thermal states. When a lower bound on $j_e(0)$ is considered, this inequality (4.3) turns out to be more restrictive than (4.2) in almost all cases, which is demonstrated by table 1 too. For better transparency we define

$$\tilde{c}_{j_e}^{lb} = \frac{6}{\pi} \frac{\langle \mathbf{j}_p \rangle_{\beta_l} - \langle \mathbf{j}_p \rangle_{\beta_r}}{(T_l^2 - T_r^2)}, \quad (4.4)$$

to compare the dynamical central charge with.

A trivial consequence of (4.2) is the bound

$$c_{IR} \leq \tilde{c}_{j_e}(T_l, T_r) \leq c_{UV}, \quad (4.5)$$

where the bounds are now independent of the temperatures, and the lower bound is less strict than the one obtained in [93]. This means that a simple estimate for $j_e(0)$ is given by

$$\frac{\pi c_{IR}}{12} (T_l^2 - T_r^2) \leq j_e(0) = \max j_e \leq \frac{\pi c_{UV}}{12} (T_l^2 - T_r^2), \quad (4.6)$$

and hence the the whole Euler scale energy current is always bounded by $\frac{\pi c_{UV}}{12} (T_l^2 - T_r^2)$.

The dynamical central charge \tilde{c}_{j_e} has another nice property; similarly to the effective central charge, this quantity is a monotonously increasing function of the energy scale. In more precise terms

$$\begin{aligned} \tilde{c}_{j_e}(T_l^{(1)}, T_r^{(1)}) \geq \tilde{c}_{j_e}(T_l^{(2)}, T_r^{(2)}) \quad & \text{if} \quad \max(T_l^{(1)}, T_r^{(1)}) \geq \max(T_l^{(2)}, T_r^{(2)}) \\ & \text{and} \quad \min(T_l^{(1)}, T_r^{(1)}) \geq \min(T_l^{(2)}, T_r^{(2)}) \end{aligned} \quad (4.7)$$

and

$$\begin{aligned} \tilde{c}_{j_e}(T_l^{(1)}, T_r^{(1)}) \geq \tilde{c}_{j_e}(T_l^{(2)}, T_r^{(2)}) \quad & \text{if} \quad \min(T_l^{(1)}, T_r^{(1)}) \geq \min(T_l^{(2)}, T_r^{(2)}) \\ & \text{and} \quad \max(T_l^{(1)}, T_r^{(1)}) = \max(T_l^{(2)}, T_r^{(2)}) . \end{aligned} \quad (4.8)$$

A monotonic behaviour of \tilde{c}_{j_e} was first pointed out in [92]. However, the validity of the approach used to determine the NESS in that particular work was not justified by later comparison with the GHD [42], although the difference between the numerical values was small. Our analysis relying on the GHD approach now gives solid evidence for the monotonicity of \tilde{c}_{j_e} in terms of (4.7) and (4.8).

Based on eq. (1.1), nevertheless, an effective central charge can be defined not only from j_e , but also from q_e and j_p , which are not equal due to the lack of exact conformal symmetry in massless models. Again, it seems reasonable to chose their value at the ray $\xi = 0$, which corresponds to the NESS, but it is important to keep in mind that for these quantities their maximum does not occur at $\xi = 0$. Defining the corresponding dynamical central charges denoted them by \tilde{c}_{q_e} and \tilde{c}_{j_p} their numerical values can be determined as seen in table 1. As indicated by table 1 similar observation can be made to the case of \tilde{c}_{j_e} , which we summarise as follows: for \tilde{c}_{j_p}

$$c_{IR} \leq \tilde{c}_{j_p}(T_l, T_r) \leq \tilde{c}_{j_e}(T_l, T_r) \quad (4.9)$$

holds, from which it also follows that

$$c_{IR} \leq \tilde{c}_{j_p}(T_l, T_r) \leq c_{UV} . \quad (4.10)$$

On the contrary for \tilde{c}_{q_e} we find that

$$c_{IR} \leq \tilde{c}(\max(T_l, T_r)) \leq \tilde{c}_{q_e}(T_l, T_r) \lesssim c_{UV} . \quad (4.11)$$

In this formula the symbol \lesssim before c_{UV} seems very unnatural first. Even though the problematic numerical values for \tilde{c}_{q_e} (i.e. those slightly large than 0.7) seem to be stable against varying the parameters in the numerical solutions (such as the number of iterations or discretisation points etc.) we cannot exclude the possibility of numerical errors and therefore leave this problem open. Nevertheless it is important to remember that q_e has no global extremum at $\xi = 0$ and in the rest of the paper we present an interesting argument stating that unlike for currents such an anomalous behaviour is not prohibited by physical principles for densities (apart from the $T^{(l)}, T^{(r)} \rightarrow 0$ and $T^{(l)}, T^{(r)} \rightarrow \infty$ limits where the CFT description becomes exact).

In the next section it is also demonstrated that the conjectures (4.2), (4.9) and (4.11) and the monotonicity property (4.7), (4.8) for \tilde{c}_{j_e} remain valid for the other flows of the A_n and D_n family together with the extended plateaux in the current and density profiles.

4.2 Low energy behaviour and constant regions in the density/current profiles in the A_2 flow

As indicated by figure 1, for low and intermediate left and right temperatures, there are regions of the ray ξ where the densities and currents have constant values. To understand

the emergence of such regions, it is useful to remember that the bare velocities of the RM and LM particles are ± 1 and in macro-states (either homogeneous or inhomogeneous) the interactions changes the range of the effective velocities from ± 1 to $[v_{RM}^{min}, 1]$ and $[-1, v_{LM}^{max}]$. The appearance of the flat regions in the density and current profiles is related the fact that at not too high temperatures these intervals do not overlap. This means that, according to our discussion at the end of section 2.2,

$$\begin{aligned} n_{RM}(\vartheta, \xi) &= n_{RM}^{(l)}(\vartheta) \\ n_{LM}(\vartheta, \xi) &= n_{LM}^{(r)}(\vartheta) \end{aligned} \quad \text{if } \xi \in [v_{LM}^{max}, v_{RM}^{min}], \quad (4.12)$$

which are independent of ξ and consequently the current and density profiles have no ξ -dependence too. It is a notable observation that if $[v_{RM}^{min}, 1] \cap [-1, v_{LM}^{max}] = \{\}$ then $0 \in [v_{LM}^{max}, v_{RM}^{min}]$ always holds.

At very low temperatures it is also possible to treat the problem by analytical means at least in two different ways. An obvious approach is the low temperature expansion of the thermal TBA equations first. If one is interested in the flat regions of the profiles the values of the densities and currents are straightforwardly obtained using again a low-temperature expansion in (2.6), (2.8) and (2.5) since (4.12) can be exploited.

Another approach is describing the low energy behaviour of the A_2 massless flow as an irrelevant perturbation of the IR CFT by $\int d^2x T\bar{T}$ [94, 95]. In particular for the A_2 , model the low-energy effective Lagrangian reads [80, 94]

$$\mathcal{L}_{eff} = \psi\bar{\partial}\psi + \bar{\psi}\partial\bar{\psi} - \frac{4}{M^2}(\psi\partial\psi)(\bar{\psi}\bar{\partial}\bar{\psi}) + \dots, \quad (4.13)$$

where $\psi\bar{\partial}\psi + \bar{\psi}\partial\bar{\psi}$ is the Lagrangian of the critical Ising field theory with $c = \frac{1}{2}$ and

$$\begin{aligned} T &= -\frac{1}{2}\psi\partial\psi \\ \bar{T} &= -\frac{1}{2}\bar{\psi}\bar{\partial}\bar{\psi}. \end{aligned} \quad (4.14)$$

The bipartite quench with left and right thermal heat reservoirs was analysed in [72] for perturbed CFTs with the action

$$S = S_{CFT} + g \int d^2x T\bar{T}. \quad (4.15)$$

In particular, the average of the energy and momentum densities and currents are modified by the perturbation [72] from eq. (1.1) to

$$\begin{aligned} q_e &= \frac{c\pi}{12} \left[T_l^2 + T_r^2 - \frac{gc\pi}{12} (T_l^4 + T_r^4 + T_l^2 T_r^2) \right] + \mathcal{O}(g^2) \\ j_e = q_p &= \frac{c\pi}{12} \left[T_l^2 \left(1 - \frac{gc\pi}{12} T_l^2 \right) - T_r^2 \left(1 - \frac{gc\pi}{12} T_r^2 \right) \right] + \mathcal{O}(g^2) \\ j_p &= \frac{c\pi}{12} \left[T_l^2 + T_r^2 - \frac{gc\pi}{12} (T_l^4 + T_r^4 - T_l^2 T_r^2) \right] + \mathcal{O}(g^2) \end{aligned} \quad (4.16)$$

and the velocities for the shock waves v_{LM}^{max} and v_{RM}^{min} are

$$\begin{aligned} v_{LM}^{max} &= -1 - \frac{gc\pi}{12} T_l^2 + \mathcal{O}(g^2) \\ v_{RM}^{min} &= 1 + \frac{gc\pi}{12} T_r^2 + \mathcal{O}(g^2). \end{aligned} \quad (4.17)$$

Substituting $-\frac{16}{M^2}$ for g according to eqs. (4.16) and (4.17) and trading the small parameter to T^2 , the results obtained describe the low temperature Euler scale behaviour of the A_2 flow:

$$\begin{aligned} q_e &= \frac{\pi}{24} \left[T_l^2 + T_r^2 + \frac{2\pi}{3} (T_l^4 + T_r^4 + T_l^2 T_r^2) \right] + \mathcal{O}(T^6) \\ j_e = q_p &= \frac{\pi}{24} \left[T_l^2 \left(1 + \frac{2\pi}{3} T_l^2 \right) - T_r^2 \left(1 + \frac{2\pi}{3} T_r^2 \right) \right] + \mathcal{O}(T^6) \\ j_p &= \frac{\pi}{24} \left[T_l^2 + T_r^2 + \frac{2\pi}{3} (T_l^4 + T_r^4 - T_l^2 T_r^2) \right] + \mathcal{O}(T^6) \end{aligned} \quad (4.18)$$

for $\xi \in [v_{LM}^{max}, v_{RM}^{min}]$, where

$$\begin{aligned} v_{LM}^{max} &= -1 + \frac{2\pi}{3} T_l^2 + \mathcal{O}(T^4) \\ v_{RM}^{min} &= 1 - \frac{2\pi}{3} T_r^2 + \mathcal{O}(T^4). \end{aligned} \quad (4.19)$$

An alternative derivation of these results is given in appendix A by performing the low temperature expansion of the TBA equations (2.5), (2.6), (2.8) and (2.10).

Finally, it is important to note that for the particular case of the A_2 flow no shocks develop due to integrability contrary to the general case of the $T\bar{T}$ perturbation [72].

5 Hydrodynamics of the A_n and D_n flows

Now we turn to studying higher members of the A_n and also D_n type massless models, which correspond to the Dynkin diagrams in figure 1.

In figure 5 the density and current profiles for the A_3 flow are displayed for various left and right initial temperatures. The model can be regarded as the RG trajectory from the tetra-critical to the tricritical Ising field theory with $c_{UV} = 0.8$ and $c_{IR} = 0.7$, and for this model the TBA equations also include a magnonic particle. Figure 5 shows a behaviour similar to the case of the A_2 flow: irrespectively of the left and right temperatures the profiles include extended plateaux and in fact the flat regions are even broader than in the previous case. For the A_2 model an explanation for the plateaux was given based on the high- and low-temperature conformal behaviour and also on the qualitative behaviour of GHD and TBA equations. To give an explanation for the plateaux for this case and eventually for all higher members of the A_n flow it is sufficient to note that the difference between the IR and UV central charges decreases as n increases (3.4). This means that the UV and

IR CFTs only slightly differ from each other as long as the number of effective degrees of freedom or the transport properties determined by the central charge are concerned. Thus the properties of the interpolating flow are expected to be similar to the CFT case including the appearance of the plateaux. In this respect, the A_2 case is the one expected to show the largest departure from the CFT behaviour since it is for this case that the difference between the UV and IR central charges is the largest.

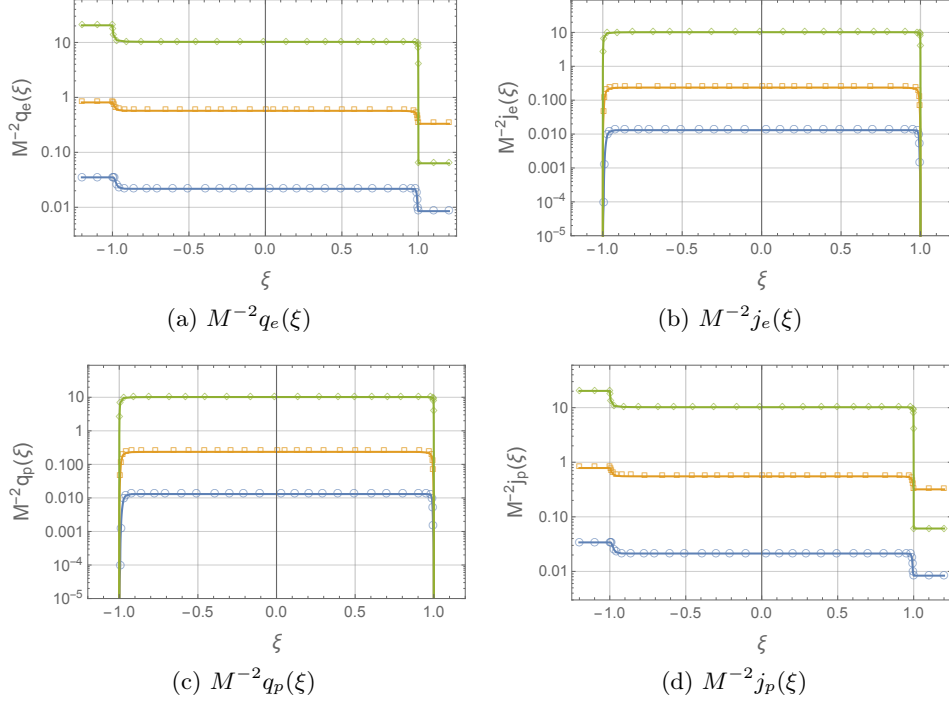


Figure 5: Ray-dependent (a) energy density q_e , (b) energy current j_e , (c) momentum density q_p and (d) momentum current j_p in the A_3 (tetra-critical to tricritical Ising) and D_3 flow after bipartite quenches at the Euler scale. The green curve with diamonds corresponds to left and right initial temperatures $T_l = 7M$ and $T_r = 0.4M$, the orange curve with squares to $T_l = 1.4M$ and $T_r = 0.9M$ and the blue curve with circles to $T_l = 0.3M$ and $T_r = 0.15M$. The discrete points in the plots indicated by the plotmarkers are obtained by the numerical solution of GHD equations, the continuous curves are first order interpolations. Due to relativistic invariance, $j_e = q_p$.

It is worth noting that unlike for the A_2 for the A_3 flow (and also for higher members as one expects) the exactly flat constant regions in the profiles do not appear. Although at low temperatures the range of effective velocities for RM and LM particles do not overlap and consequently their filling functions become independent of ξ , the range of the effective velocity for the magnons spans this non-overlapping region and $n_M(\vartheta, \xi)$ has real ray-dependence. Even though the contribution to the densities and currents originates from only the RM and LM particles, the ray-dependence of $n_M(\vartheta, \xi)$ is transmitted to the densities and currents due to the dressing equation (2.5). This accounts for a weak ray-dependence in the profiles in the non-overlapping region in the range of the RM and LM effective velocities.

At sufficiently small temperatures the effective velocities for magnons also do not overlap with that of the RM or LM particles. It is a general observation the even in this case the range of the magnonic effective velocity (at least for one magnonic species) always touches the lower and upper endpoints of the range of the RM and LM effective velocities.

T_l/M	T_r/M	$\tilde{c}(T_l)$	$\tilde{c}(T_r)$	$\tilde{c}_{j_e}(T_l, T_r)$	$\tilde{c}_{q_e}(T_l, T_r)$	$\tilde{c}_{j_p}(T_l, T_r)$	$\tilde{c}_{j_e}^{lb}(T_l, T_r)$
0.2	0.1	0.713424	0.704842	0.726069	0.724252	0.714633	0.716494
0.25	0.1	0.717545	0.704842	0.730977	0.729825	0.720382	0.720142
0.3	0.15	0.721433	0.709139	0.738176	0.736503	0.722257	0.725665
0.9	0.1	0.751467	0.704842	0.766027	0.767382	0.761988	0.752054
0.9	0.85	0.751467	0.749811	0.778166	0.779638	0.750716	0.765082
0.95	0.9	0.753023	0.751467	0.779363	0.781042	0.752307	0.76658
1.4	0.9	0.763667	0.751467	0.783582	0.786193	0.76077	0.772155
2.9	1.1	0.779635	0.75717	0.790933	0.794089	0.778236	0.783189
6.5	6	0.790221	0.789469	0.796616	0.799242	0.789463	0.793952
7	0.4	0.790867	0.728439	0.794791	0.796047	0.792994	0.790611
7	6	0.790867	0.789469	0.796669	0.799237	0.789854	0.794116
9	8.5	0.792724	0.792344	0.796894	0.799172	0.791988	0.795059

Table 2: The effective central charges for (left and right) thermal states and the dynamical central charges for the partitioning protocol for various left and right temperatures in the A_3 and D_3 massless flows, where $c_{UV} = 0.8$ and $c_{IR} = 0.7$.

In table 2, the effective and dynamical central charges defined in eq. (4.1) are collected for different left and right temperatures in the A_3 interpolating flow, and the data confirm that the conjecture (4.2) proposed for the A_2 massless flow remains valid in the present case. Therefore it is plausible to assume that together with the appearance of the plateaux in the profile, the conjectures (4.2), (4.9) and (4.11) for the dynamical central charges and the bounds for the currents are a general property of the A_n models in the thermal partitioning protocol.

In fact the broad plateaux in the profiles and the conjectures (4.2)-(4.11) seem to be a generic property of not only the A_n massless models, but also of the D_n series and eventually of all unitary massless integrable flows. This is confirmed by studying the first two members of the D_n series. What concerns the D_3 flow it is to mention that its TBA system is equivalent with that of the A_3 model. Though the operator content and consequently the models themselves are different, the energy and momentum densities and currents are given by the same equations and figure 5 and table 2 describes both the A_3 and D_3 flows. Another notable remark is that the \mathbb{Z}_3 parafermion model, i.e. the UV limiting theory of the D_3 model is the critical three-state Potts model.

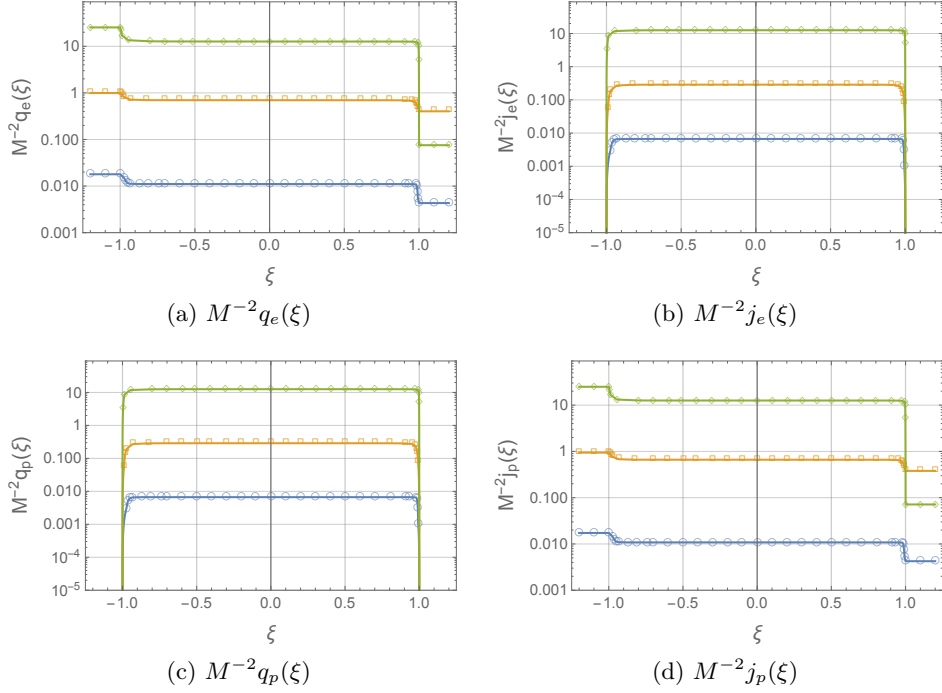


Figure 6: Ray-dependent (a) energy density q_e , (b) energy current j_e , (c) momentum density q_p and (d) momentum current j_p in the D_4 flow after bipartite quenches at the Euler scale. The green curve with diamonds corresponds to left and right initial temperatures $T_l = 7M$ and $T_r = 0.4M$, the orange curve with squares to $T_l = 1.4M$ and $T_r = 0.9M$ and the blue curve with circles to $T_l = 0.2M$ and $T_r = 0.1M$. The discrete points in the plots indicated by the plotmarkers are obtained by the numerical solution of GHD equations, the continuous curves are first order interpolations. Due to relativistic invariance, $j_e = q_p$.

Figure 6 and table 3 show the ray-dependent energy and momentum density and current profiles and the values of effective and dynamical central charges. For the D_n series the $n \rightarrow \infty$ limit the difference of the UV and IR central charges is now 1 (3.5) and arguing that the UV and IR CFTs are 'similar' is not possible. Nevertheless, the presence of the extended plateaux and validity of the conjectures (4.2)-(4.11) in the D_4 model besides the D_3 case suggest that these features emerge in any member of the D_n flows.

Whereas tables 2 and 3 suggest that the approximate inequality in (4.11) is rather a strict one, studying the hydrodynamics of massless perturbation of the W_5^3 CFT (carried out in appendix B) slightly larger than c_{UV} values for \tilde{c}_{q_e} can be seen again. Our analysis is therefore not conclusive in the question whether $c_{UV} \geq \tilde{c}_{q_e}$ or $c_{UV} \gtrsim \tilde{c}_{q_e}$ holds for finite and non-zero left and right temperatures but we revisit this issue in the next section.

T_l/M	T_r/M	$\tilde{c}(T_l)$	$\tilde{c}(T_r)$	$\tilde{c}_{j_e}(T_l, T_r)$	$\tilde{c}_{q_e}(T_l, T_r)$	$\tilde{c}_{j_p}(T_l, T_r)$	$\tilde{c}_{j_e}^{lb}(T_l, T_r)$
0.2	0.1	0.824632	0.808665	0.847828	0.844655	0.826961	0.830546
0.6	0.1	0.87268	0.808665	0.900474	0.902396	0.889841	0.874614
1.1	0.1	0.905374	0.808665	0.93072	0.933312	0.924594	0.905972
1.1	0.9	0.905374	0.894632	0.950457	0.954026	0.901267	0.926701
1.4	0.9	0.917764	0.894632	0.955841	0.960591	0.912188	0.933531
2.9	1.1	0.949132	0.905346	0.971613	0.977795	0.946437	0.955505
6.5	6.0	0.971295	0.969662	0.985085	0.991036	0.968856	0.978339
7	0.4	0.972897	0.852085	0.980875	0.983581	0.977281	0.971403
7	6	0.972707	0.969662	0.985222	0.991092	0.969695	0.978704
9	8.5	0.976816	0.975969	0.98579	0.991373	0.974226	0.980793

Table 3: The effective central charges for (left and right) thermal states and the dynamical central charges for the partitioning protocol for various left and right temperatures in the D_4 massless flow, where $c_{UV} = 1$ and $c_{IR} = 0.8$.

6 The Landauer-Büttiker picture and its implications on transport

In this section, we would like to discuss a simple physical picture that gives a natural interpretation for the observed bounds for the dynamical central charges and provides a possible explanation for the anomalous behaviour of \tilde{c}_{q_e} . This picture is based on the Landauer-Büttiker (LB) formalism [96–99] of electronic systems, which claims that in the simplest case the total electric conductance for 1D systems with ballistic electron propagation is the number of open channels for the electrons times the conductance quantum $2e^2/h$. The prototypical case where this formalism is used is a clean quantum wire supporting coherent propagation of electronic excitations attached to a source and a drain with an applied voltage emitting and absorbing electrons according to Fermi-Dirac statistics. It is easy to use the LB formalism to describe thermal transport when the temperatures of the drain and the source are different. For the energy current of relativistic and spinless fermions with mass m elementary calculations give

$$\mathcal{J}(T_l) - \mathcal{J}(T_r) \quad (6.1)$$

with

$$\mathcal{J}(T) = \frac{T^2 \left[\pi^2 - 3\frac{m^2}{T^2} + \frac{6m}{T} \log(1 + e^{m/T}) + 6\text{Li}_2(-e^{m/T}) \right]}{12\pi} \quad (6.2)$$

whose $m \rightarrow 0$ limit, which is the conformal limit, yields

$$\frac{1}{2} \frac{\pi}{12} (T_l^2 - T_r^2), \quad (6.3)$$

i.e. the CFT result. Whereas this result is obtained for the case of non-interacting quasi-particles and it is not obvious how the LB formalism could be applied for general CFTs,

the connection between the LB formalism and the CFT treatment in the free case inspires the following interpretation for the CFT current formula: the central charge simply counts the number of open channels for the energy transport. This statement is in agreement with usual interpretation of the central charge counting the number of effective degrees of freedom in the theory.

If one accepts this picture linking the central charge and the number of open channels for the energy transport, the existence of both an upper and a lower bound for the dynamical central charge \tilde{c}_{j_e} in massless flows comes naturally. The number of effective degrees of freedom in massless models cannot be larger than c_{UV} and smaller than c_{IR} and consequently the number of open channels available for energy transport must be bounded by c_{UV} and c_{IR} too. Clearly, the same argument holds also for the current of the momentum.

Even if the transport is ballistic and an upper bound for the conductance is expected, the accumulation of charge is not prohibited, at least by our simple picture. In our analysis the problematic quantity with respect to an upper bound was the average energy density at $\xi = 0$, which is a density of a conserved charge and hence is compatible with the previous statements. Due to relativistic invariance $j_e = q_p$, which explains why anomalous behaviour could be detected only for q_e .

The formulae (6.1) and (6.2) were derived for massive relativistic fermions, which means that c_{IR} equals zero. Analysing the behaviour of the dynamical central charge \tilde{c}_{j_e} for the energy current (6.1), it is easy to check that it is indeed bounded by 0 and 1/2 in accordance with the above interpretation and that $c_{IR} = 0$. Due to the exact expression for \tilde{c}_{j_e} , nevertheless, its monotonicity properties can also be explicitly investigated and (4.7) and (4.8) are satisfied. For this property, which is therefore valid for massless flows as well as relativistic fermions in the LB picture, the interpretation is also at hand. Increasing the temperature in any of the initial subsystems results in higher energy densities and a larger number of open channels available for the energy transport since in unitary theories the number of effective degrees of freedom is increased with increased energy density. Whereas it remains an assumption that the number of open channels for transport is a monotonous function of the number of effective degrees of freedom as it happens for free fermions, thinking in terms of the stable quasi-particles of integrable systems with ballistic propagation makes this link very plausible.

Having seen how the LB picture can explain some of the observed bounds for the dynamical central charges together with the monotonicity of \tilde{c}_{j_e} in massless integrable models and massive free fermions, it is natural to speculate about the case of massive integrable and eventually general 1+1D QFTs. For this reason we also analyse the dynamical central charges in the sinh-Gordon model using the GHD and the partitioning protocol again. Without explaining too many details about the model (in connection with GHD this model was investigated in [42] reviewing its definition) we merely quote the corresponding TBA equation containing one single particle species:

$$\varepsilon(\vartheta) = \frac{m \cosh(\vartheta)}{T} - (\varphi_{shG} \star \ln(1 + e^{-\varepsilon}))(\vartheta), \quad (6.4)$$

with

$$\varphi_{shG}(\vartheta) = -\frac{4 \cosh(\vartheta) \sin(\frac{B\pi}{2})}{\cos(B\pi) - \cosh(2\vartheta)}, \quad (6.5)$$

where m is particle mass and the parameter B takes values from $[0, 2]$ and is related to the strength of the interaction.

T_l/M	T_r/M	$\tilde{c}(T_l)$	$\tilde{c}(T_r)$	$\tilde{c}_{j_e}(T_l, T_r)$	$\tilde{c}_{q_e}(T_l, T_r)$	$\tilde{c}_{j_p}(T_l, T_r)$	$\tilde{c}_{j_e}^{lb}(T_l, T_r)$
0.2	0.04	0.0122958	0	0.0255886	0.0681836	0.0118277	0.0128082
0.2	0.1	0.0122958	0.00011	0.0326524	0.0569543	0.00986332	0.0163566
0.5	0.1	0.172818	0.00011	0.263287	0.444249	0.167334	0.180014
0.5	0.3	0.172818	0.054912	0.342032	0.397678	0.142199	0.23914
0.6	0.1	0.227963	0.000113	0.326837	0.521414	0.223859	0.234473
0.6	0.3	0.227963	0.054912	0.392442	0.473548	0.194677	0.285647
1.2	0.1	0.447465	0.000113	0.546621	0.721098	0.452063	0.450593
1.2	0.6	0.447465	0.227963	0.619103	0.698749	0.406992	0.520632
7	3.5	0.789094	0.695874	0.855191	0.884953	0.773724	0.820188
7	6	0.789094	0.771895	0.867738	0.892567	0.782	0.836757
8	0.6	0.802629	0.227963	0.842828	0.878939	0.813516	0.805906
8	6	0.802629	0.771895	0.871823	0.895377	0.792172	0.842194

Table 4: The effective central charges for (left and right) thermal states and the dynamical central charges for the partitioning protocol for various left and right temperatures in the massive sinh-Gordon theory with $B = 0.5$, where $c_{UV} = 1$ and $c_{IR} = 0$.

Table 4 shows the data for the effective and dynamical central charges for the sinh-Gordon model and the data are in perfect agreement with the predictions of the LB picture. All the dynamical central charges are bounded by c_{IR} from below and for the currents (and in this case also for q_e) the data are consistent with an upper bound given by c_{UV} , and the monotonicity property of \tilde{c}_{j_e} is also satisfied. Moreover, the conjectures (4.2), (4.9) and (4.11) proposed for the massless models also hold in this case together with (4.3), whose validity is independent of the massless or massive nature of the theory.

Although a systematic treatment of the hydrodynamics in massive integrable QFTs is out of the scope of this paper, based on the above results it is plausible to expect that the bounds for the dynamical central charges of currents given by c_{IR} and c_{UV} , the monotonicity of \tilde{c}_{j_e} and the conjectures (4.2), (4.9) and (4.11) are valid in any relativistic and unitary integrable QFT and the interpretation inspired by the LB picture is correct. The monotonic behaviour of \tilde{c}_{j_e} is an especially interesting finding, since it corresponds to an out-of-equilibrium version of the well-known c-theorem.

In fact, considering a generic unitary and relativistic 1+1 D QFT with homogeneous bulk action it is reasonable to assume that the dynamical central charges of the energy and momentum current are still bounded by c_{UV} from above and c_{IR} from below. In non-integrable cases there are usually no additional conserved quantities to the energy and the momentum and the ray-dependent profiles for the currents and densities of these

conserved quantities can exhibit discontinuities at the Euler scale. Nevertheless the NESS corresponding to $\xi = 0$ at the Euler scale is expected to be well defined and therefore the dynamical central charges can be introduced similarly to the integrable case. Whether the strict monotonicity property of \tilde{c}_{je} alias a non-equilibrium c-theorem holds in non-integrable cases is a more subtle issue. Whereas the c-function [89] in eq. (2.15) was defined via the TBA and hence exists only for Bethe Ansatz integrable models, a c-function with the same monotonicity property was first defined from the two-point function of the stress-energy tensor [88]. This function can be ascribed to the same interpretation as the TBA c-function i.e. counting the number of effective degrees of freedom but it can be defined for any 1+1 D perturbed CFT and accordingly the equilibrium c-theorem is valid in any field theory of this type. Although its monotonicity suggests a monotonic behaviour for \tilde{c}_{je} , due to the inelastic scattering between particles, the possible particle production processes and the absence of ballistic propagation it is difficult to give evidence and to reduce the uncertainty left. We therefore leave this question open, which we hope to be the subject of further studies.

7 Conclusions

In this paper we studied the Euler scale hydrodynamics of massless integrable quantum field theories (QFTs) in the partitioning protocol using the recently developed framework of generalised hydrodynamics (GHD) [42–44]. The peculiarity of these models is that they interpolate between two non-trivial renormalisation group fixed points corresponding to conformal field theories (CFTs) with a crossover from one CFT to another characterised by an energy scale called crossover scale. In particular we calculated the Euler scale current and density profiles for the energy and momentum after joining the semi-infinite left and right halves of the massless systems initially prepared to different thermal states. Focusing on the first few members of the A_n and D_n massless flows, we carried out a systematic treatment of the A_n and D_n series.

Our analysis identified some general characteristic features regarding the transport properties of these massless flows. Irrespectively of the magnitude of the left and right temperatures with respect to the crossover scale of the massless theory, the density and current profiles exhibit extended plateaux in the non-trivial region $\xi \in [-1, 1]$, where ξ stands for x/t sending x and t to infinity. This behaviour is similar to the case of CFTs, whose profiles contain constant regions separated by discontinuous jumps at $\xi = \pm 1$ in the Euler limit [69, 70], but integrability prevents the formation of such discontinuities and shock-waves in massless flows. The presence of discontinuities in the CFT profiles and their absence in the integrable massless case might seem surprising given that rational CFTs are eventually integrable models having infinitely many local conserved quantities. The main difference between these theories accounting for the different behaviour is the existence of particles with non-trivial dispersion in integrable cases, whereas in CFTs the propagation of modes is dispersionless, which can thus accumulate to form shock-waves.

We analysed the magnitude of the currents and densities and constructed a series of bounds for them at ray $\xi = 0$, which corresponds to the non-equilibrium stationary state

(NESS) that is when $t \rightarrow \infty$ but x remains finite. Simple upper and lower bounds for the energy current can be given using the CFT result (1.1) with central charge of the UV and IR limiting CFTs respectively and the initial left and right temperatures. We also showed the dynamical central charge \tilde{c}_{j_e} defined in eq. (4.1) inspired by writing the maximum of the energy current in form of the CFT energy current is bounded from below by not only the central charge of the IR limiting CFT but by the effective central charges (2.15) of the massless model corresponding to the left and right temperatures. In [93] a different lower bound was given for the energy current in the NESS or for the corresponding dynamical central charge. Our data are consistent with this lower bound, which in almost all cases turned out to be even more restrictive than the one resulting from the effective central charges. It is worth mentioning that the value of the energy current in the NESS is equal to its absolute maximum, therefore the upper bound for $j_e(0)$ is an upper bound for j_e at any ray. We also verified, that the dynamical central charge \tilde{c}_{j_e} satisfies a particular monotonicity property first discussed in [92], which resembles the usual effective central charge.

Similarly to the energy current we defined dynamical central charges \tilde{c}_{q_e} and \tilde{c}_{j_p} for the energy density q_e and for the momentum current j_p using their values in the NESS and corresponding CFT formula (1.1). For \tilde{c}_{j_p} a lower bound is given by c_{IR} and an upper bound by \tilde{c}_{j_e} whereas for \tilde{c}_{q_e} only a lower bound could be given by \tilde{c}_{j_e} , as its value can occasionally be larger than c_{UV} .

All these observations are based on the explicit investigation of the A_2 , A_3 , D_3 and D_4 models and on the massless flow from the W_5^3 to the W_4^3 CFTs and their validity is very plausible for any member of the A_n and D_n flow and eventually in any unitary massless models. The emergence of the extended plateaux is easy to understand in the low- and high-temperature limits as in these cases the CFT description of the massless model becomes valid and for intermediate temperatures a simple argument was given based on the TBA equations and neglecting magnonic particles in section 4.

Regarding the peculiar properties of the currents and densities we discussed the Landauer-Büttiker formalism of ballistic transport and its applicability to the free fermion CFT in the partitioning protocol. This connection suggest that the dynamical central charges for the currents count the number of open channels for transport and also accounts for the extremal upper and lower bounds given by c_{IR} and c_{UV} . This picture, however, does not prohibit the accumulation of charge and can be compatible with the observed behaviour of \tilde{c}_{q_e} . Using this picture it is also possible to argue for the monotonicity property of \tilde{c}_{j_e} . These predictions do not depend on the massless and massive nature of the integrable theory and were indeed found valid for the massive sinh-Gordon model together with the other bounds discussed in the previous paragraphs. The bounds, and the predictions coming from the Landauer-Büttiker picture such as the extremal bounds and the monotonicity of \tilde{c}_{j_e} corresponding to a non-equilibrium c-theorem are therefore likely to be valid in any 1+1 D relativistic integrable QFT. A further notable implication of the argument based upon the Landauer-Büttiker formalism is that for any low dimensional perturbed conformal field theory universal upper and lower bounds exist for the energy and momentum currents in the NESS. These bounds are given by c_{UV} and c_{IR} i.e. the central charge of the UV limiting

CFT and the IR limiting CFT when $c_{IR} \neq 0$. The $c_{IR} = 0$ case corresponds to massive theories, whose low-energy properties are not described by a CFT. This statement should also hold in near critical systems as long as the temperatures are not too large to spoil the effective field theory description.

Finally, for the particular case of the A_2 flow, which corresponds to the massless flow from the tricritical to the critical Ising model, interesting low-temperature transport properties were observed: in this case exactly constant regions appear in the profiles although at the same time they become smooth functions contrary to the CFT limit. The origin of this phenomenon is related to the existence of additional (temperature-dependent) bounds for the effective velocities of massless particles besides the speed of light, and the exactly flat regions emerge in any massless integrable models without magnons as demonstrated by the $W_5^3 \rightarrow W_4^3$ flow in appendix B. For the particular case of the A_2 whose low-energy limit can be described by a $T\bar{T}$ perturbation of the IR CFT, we checked our results against the prediction of [72].

Our work leaves many interesting open directions for further exploration. The current formulation of GHD uses the language of TBA but for many integrable models the non-linear integral equation (NLIE) [100–107] provides an alternative way to extract thermal (or equivalently finite volume) properties. It is therefore tempting to try to generalise the NLIE to be able to describe inhomogeneous situations. The applicability of a generalised NLIE would be especially valuable for models with a nested Bethe Ansatz. An important example is the sine-Gordon theory for general coupling, whose TBA system has infinitely many magnons, whereas the its NLIE description is much simpler. As for many massless models, such as the A_n series, the NLIEs are known they provide an ideal playground to develop an ‘inhomogeneous NLIE’ because of their simple transport properties to crosscheck the NLIE results with.

The NLIE would be also helpful when analysing the flows associated with the exceptional Lie algebras as their TBA system contains several magnons and the numerical solution of the GHD equations can become very tedious. Another interesting potential application is to non-unitary flows such as the T_n series of models. For many non-unitary flows that the effective central charge has a non-monotonic behaviour [103], which may have interesting implications for the transport properties of the system.

Finally, it would be interesting to study if the Landauer-Büttiker picture can explain the other observed bounds for the dynamical central charges and to explore if some of its implications together with the out-of-equilibrium version of the c-theorem remain valid in non-integrable relativistic and low dimensional quantum field theories.

Acknowledgements

I am grateful to Benjamin Doyon, Bruno Bertini and Márton Kormos for useful discussions and to Gábor Takács for his valuable comments and suggestions such as to investigate the connection with the Landauer-Büttiker picture. I am also indebted to Márton Kormos for useful comments and to Gábor Takács for carefully reading the manuscript.

This research was supported by the National Research Development and Innovation Office (NKFIH) under K-2016 grant no. 119204 and by the BME-Nanotechnology FIKP

grant of EMMI (BME FIKP-NAT).

References

- [1] T. Kinoshita, T. Wenger, and D. S. Weiss, *Nature* **440** (2006) 900–903.
- [2] S. Trotzky, Y.-A. Chen, A. Flesch, I. P. McCulloch, U. Schollwöck, J. Eisert and I. Bloch, *Nature Phys.* **8** (2012) 325–330, arXiv:1101.2659 [cond-mat.quant-gas].
- [3] M. Gring, M. Kuhnert, T. Langen, T. Kitagawa, B. Rauer, M. Schreitl, I. Mazets, D. A. Smith, E. Demler and J. Schmiedmayer, *Science* **337** (2012) 1318–1322, arXiv:1112.0013 [cond-mat.quant-gas].
- [4] T. Langen, S. Erne, R. Geiger, B. Rauer, T. Schweigler, M. Kuhnert, W. Rohringer, I. E. Mazets, T. Gasenzer and J. Schmiedmayer, *Science* **348** (2015) 207–211, arXiv:1411.7185 [cond-mat.quant-gas].
- [5] S. Hofferberth, I. Lesanovsky, B. Fischer, T. Schumm and J. Schmiedmayer, *Nature* **449**, 324 (2007), arXiv:0706.2259 [cond-mat.other].
- [6] T. Langen, R. Geiger, M. Kuhnert, B. Rauer and J. Schmiedmayer, *Nature Physics* **9**, 640 (2013), arXiv:1305.3708 [cond-mat.quant-gas].
- [7] F. Meinert, M. J. Mark, E. Kirilov, K. Lauber, P. Weinmann, A. J. Daley and H.-C. Nägerl, *Phys. Rev. Lett.* **111** (2013) 053003, arXiv:1304.2628 [cond-mat.quant-gas].
- [8] T. Fukuhara, P. Schauß, M. Endres, S. Hild, M. Cheneau, I. Bloch and C. Gross, *Nature* **502** (2013) 76, arXiv:1305.6598 [cond-mat.quant-gas].
- [9] A. M. Kaufman, M. E. Tai, A. Lukin, M. Rispoli, R. Schittko, P. M. Preiss and M. Greiner, *Science* **353** (2016) 794, arXiv:1603.04409 [quant-ph].
- [10] M. Cheneau, P. Barmettler, D. Poletti, M. Endres, P. Schauss, T. Fukuhara, C. Gross, I. Bloch, C. Kollath and S. Kuhr, *Nature* **481** (2012) 484–487, arXiv:1111.0776 [cond-mat.quant-gas].
- [11] P. Calabrese and J. Cardy, *Phys. Rev. Lett.* **96** (2006) 136801, arXiv:cond-mat/0601225.
- [12] P. Calabrese and J. Cardy, *J. Stat. Mech.* **0706** (2007) P06008, arXiv:0704.1880 [cond-mat.stat-mech].
- [13] M. Rigol, V. Dunjko, V. Yurovsky and M. Olshanii, *Phys. Rev. Lett.* **98** (2007) 050405, arXiv:cond-mat/0604476 [cond-mat.other].
- [14] A. C. Cassidy, C. W. Clark and M. Rigol, *Phys. Rev. Lett.* **106** (2011) 140405, arXiv:1008.4794 [cond-mat.stat-mech].
- [15] B. Pozsgay, *J. Stat. Mech.* **1101** (2011) P01011, arXiv:1009.4662 [hep-th].
- [16] B. Wouters, J. De Nardis, M. Brockmann, D. Fioretto, M. Rigol and J.-S. Caux, *Phys. Rev. Lett.* **113** (2014) 117202, arXiv:1405.0172, arXiv:1405.0172 [cond-mat.str-el].
- [17] B. Pozsgay, M. Mestyán, M. A. Werner, M. Kormos, G. Zaránd and G. Takács, *Phys. Rev. Lett.* **113** (2014) 117203, arXiv:1405.2843 [cond-mat.stat-mech].
- [18] B. Pozsgay, *J. Stat. Mech.* **9** (2014) 09026, arXiv:1406.4613 [cond-mat.stat-mech].
- [19] G. Goldstein and N. Andrei, *Phys. Rev. A* **90** (2014) 043625, arXiv:1405.4224 [cond-mat.quant-gas].

- [20] F. H. L. Essler, G. Mussardo and M. Panfil, *Phys. Rev. A* **91** (2015) 051602, arXiv:1411.5352 [cond-mat.quant-gas].
- [21] E. Ilievski, J. De Nardis, B. Wouters, J.-S. Caux, F. H. L. Essler and T. Prosen, *Phys. Rev. Lett.* **115** (2015) 157201, arXiv:1507.02993 [quant-ph].
- [22] M. Mestyan, B. Pozsgay, G. Takacs and M. A. Werner, *J. Stat. Mech.* **1504** (2015) 04001 arXiv:1412.4787 [cond-mat.stat-mech].
- [23] E. Ilievski, E. Quinn, J. De Nardis and M. Brockmann, *J. Stat. Mech.* **1606** (2016) 063101, arXiv:1512.04454 [cond-mat.stat-mech].
- [24] B. Pozsgay, E. Vernier and M. A. Werner, *J. Stat. Mech.* **2017** (2017) 093103, arXiv:1703.09516 [cond-mat.stat-mech].
- [25] E. Ilievski, E. Quinn and J.-S. Caux, *Phys. Rev. B* **95** (2017) 115128, arXiv:1610.06911 [cond-mat.stat-mech].
- [26] L. Piroli, B. Pozsgay and E. Vernier, *Nucl. Phys. B* **925**(2017) 362, arXiv:1709.04796[cond-mat.stat-mech].
- [27] E. Ilievski, M. Medenjak, T. Prosen and L. Zadnik, *J. Stat. Mech.* **1606** (2016) 064008, arXiv:1603.00440 [cond-mat.stat-mech].
- [28] T. Platini and D. Karevski, *Eur. Phys. J. B* **48** (2005) 225, arXiv:cond-mat/0509594 [cond-mat.stat-mech].
- [29] A. De Luca, J. Viti, D. Bernard and B. Doyon, *Phys. Rev. B* **88** (2013) 134301, arXiv:1305.4984 [cond-mat.str-el].
- [30] M. Collura and D. Karevski, *Phys. Rev. B* **89** (2014) 214308, arXiv:1402.1944 [cond-mat.stat-mech].
- [31] J. Viti, J.-M. Stéphan, J. Dubail and M. Haque, *EPL* **115** (2016) 40011, arXiv:1507.08132 [cond-mat.stat-mech].
- [32] A. Biella, A. De Luca, J. Viti, D. Rossini, L. Mazza and Rosario Fazio, *Phys. Rev. B* **93** (2016) 205121, arXiv:1602.05357 [cond-mat.stat-mech].
- [33] M. Fagotti, *Phys. Rev. B* **96** (2017) 220302, arXiv:1708.05383 [cond-mat.stat-mech].
- [34] M. Kormos, *SciPost Phys.* **3** (2017) 020, arXiv:1704.03744 [cond-mat.stat-mech].
- [35] G. Perfetto and A. Gambassi, *Phys. Rev. E* **96** (2017) 012138, arXiv:1704.03437 [cond-mat.stat-mech].
- [36] M. Kormos, C. P. Moca and G. Zaránd, *Phys. Rev. E* **98** (2018) 032105, arXiv:1712.09466 [cond-mat.stat-mech].
- [37] B. Doyon, J. Dubail, R. Konik and T. Yoshimura, *Phys. Rev. Lett.* **119** (2017) 195301, arXiv:1704.04151 [cond-mat.stat-mech].
- [38] V. B. Bulchandani, R. Vasseur, C. Karrasch and J. E. Moore, *Phys. Rev. Lett.* **119** (2017) 220604, arXiv:1704.03466 [cond-mat.stat-mech].
- [39] J.-S. Caux, B. Doyon, J. Dubail, R. Konik and T. Yoshimura, *Hydrodynamics of the interacting Bose gas in the Quantum Newton Cradle setup* Preprint, arXiv:1711.00873 [cond-mat.stat-mech].
- [40] M. Schemmer, I. Bouchoule, B. Doyon and J. Dubail, *Phys. Rev. Lett.* **122** (2019) 090601, arXiv:1810.07170 [cond-mat.quant-gas].

- [41] P. Ruggiero, Y. Brun and J. Dubail, *SciPost Phys.* **6** (2019) 051, arXiv:1901.08132 [cond-mat.stat-mech].
- [42] O. A. Castro-Alvaredo, B. Doyon and T. Yoshimura, *Phys. Rev.* **X 6** (2016) 041065, arXiv:1605.07331 [cond-mat.stat-mech].
- [43] B. Bertini, M. Collura, J. De Nardis and M. Fagotti, *Phys. Rev. Lett.* **117** (2016) 207201, arXiv:1605.09790 [cond-mat.stat-mech].
- [44] B. Doyon and T. Yoshimura, *SciPost Phys.* **2** (2017) 014, arXiv:1611.08225 [cond-mat.stat-mech].
- [45] L. Piroli, J. De Nardis, M. Collura, B. Bertini and M. Fagotti *Phys. Rev.* **B 96** (11) (2017) 115124, arXiv:1706.00413 [cond-mat.stat-mech].
- [46] A. De Luca, M. Collura and J. De Nardis, *Phys. Rev.* **B 96**(2) (2017) 020403, arXiv:1612.07265 [cond-mat.str-el].
- [47] E. Ilievski and J. De Nardis, *Phys. Rev.* **B 96** (2017) 081118, arXiv:1706.05931 [cond-mat.stat-mech].
- [48] M. Collura, A. De Luca and J. Viti, *Phys. Rev.* **B 97** (2018) 081111, arXiv:1707.06218 [cond-mat.stat-mech].
- [49] V. Alba, *Phys. Rev.* **B 97** (2018) 245135, arXiv:1706.00020 [cond-mat.stat-mech].
- [50] B. Bertini and L. Piroli, *J. Stat. Mech.* **1803** (2018) 033104, arXiv:1711.00519 [cond-mat.stat-mech].
- [51] V. B. Bulchandani, R. Vasseur, C. Karrasch and J. Moore, *Phys. Rev.* **B 97**(4) (2018) 045407, arXiv:1702.06146 [cond-mat.stat-mech].
- [52] A. Bastianello and A. De Luca: Integrability-protected adiabatic reversibility in quantum spin chains (2018) Preprint, arXiv:1811.07922 [cond-mat.stat-mech].
- [53] B. Doyon and H. Spohn, *J. Stat. Mech.* **1707** (2017) 073210, arXiv:1703.05971 [cond-mat.stat-mech].
- [54] X. Cao, V. B. Bulchandani and J. Moore, *Phys. Rev. Lett.* **120**(16) (2018)164101, arXiv:1710.09330 [cond-mat.stat-mech].
- [55] A. Bastianello, B. Doyon, G. Watts and T. Yoshimura, *SciPost Phys.* **4** (2018) 045, arXiv:1712.05687 [cond-mat.stat-mech].
- [56] B. Doyon: Generalised hydrodynamics of the classical Toda system (2019) Preprint, arXiv:1902.07624 [cond-mat.stat-mech].
- [57] M. Márton, B. Bertini, L. Piroli and P. Calabrese, *Phys. Rev.* **B 99** (2019) 014305, arXiv:1810.01089 [cond-mat.quant-gas].
- [58] B. Bertini, L. Piroli and M. Kormos: Transport in the sine-Gordon field theory: from generalized hydrodynamics to semiclassics (2019) Preprint, arXiv:1904.02696 [cond-mat.stat-mech].
- [59] B. Doyon, H. Spohn and T. Yoshimura, *Nucl. Phys.* **B 926** (2017) 570-582, arXiv:1704.04409 [cond-mat.stat-mech].
- [60] B. Doyon, T. Yoshimura and J.-S. Caux, *Phys. Rev. Lett.* **120** (2018) 045301, arXiv:1704.05482 [cond-mat.stat-mech].

- [61] M. Mestyán and V. Alba: **Molecular dynamics simulation of entanglement spreading in generalized hydrodynamics** (2019) Preprint, arXiv:1905.03206 [cond-mat.stat-mech].
- [62] J. Myers, M. J. Bhaseen, R. J. Harris and B. Doyon: **Transport fluctuations in integrable models out of equilibrium** (2018) Preprint, arXiv:1812.02082 [cond-mat.stat-mech].
- [63] B. Doyon and J. Myers: **Fluctuations in ballistic transport from Euler hydrodynamics** (2019) Preprint, arXiv:1902.00320 [cond-mat.stat-mech].
- [64] J. De Nardis, D. Bernard and B. Doyon, *Phys. Rev. Lett.* **121** (2018) 160603, arXiv:1807.02414 [cond-mat.stat-mech].
- [65] S. Gopalakrishnan and R. Vasseur, *Phys. Rev. Lett.* **122** (2019) 127202, arXiv:1812.02701 [cond-mat.stat-mech].
- [66] J. De Nardis, D. Bernard and B. Doyon, *SciPost Phys.* **6** (2019) 049, arXiv:1812.00767 [cond-mat.stat-mech].
- [67] A. A. Belavin, A.M. Polyakov and A.B. Zamolodchikov, *Nucl. Phys.* **B 241** (1984) 333-380.
- [68] S. Sotiriadis and J. Cardy, *J. Stat. Mech.* **0811** (2008) 11003, arXiv:0808.0116 [cond-mat.stat-mech].
- [69] D. Bernard and B. Doyon, *J. Phys.* **A 45** (2012) 362001, arXiv:1202.0239 [cond-mat.str-el].
- [70] D. Bernard and B. Doyon, *Ann. Henri Poincare* **16** (2015) 113-161, arXiv:1302.3125 [math-ph].
- [71] B. Doyon, M. Hoogeveen and D. Bernard, *J. Stat. Mech.* **1403** (2014) 03002, arXiv:1306.3192 [cond-mat.stat-mech].
- [72] D. Bernard and B. Doyon *J. Stat. Mech.* **1602** (2016) 033104, arXiv:1507.07474 [cond-mat.stat-mech].
- [73] A. Lucas, K. Schalm, B. Doyon and M. J. Bhaseen, *Phys. Rev.* **D 94** (2016) 025004, arXiv:1512.09037 [hep-th].
- [74] D. Bernard and B. Doyon, *J. Stat. Mech.* **1606** (2016) 064005, arXiv:1603.07765 [cond-mat.stat-mech].
- [75] Al. B. Zamolodchikov, *Nucl. Phys.* **B 358** (1991) 497.
- [76] Al. B. Zamolodchikov, *Nucl. Phys.* **B 358** (1991) 524.
- [77] Al. B. Zamolodchikov, *Nucl. Phys.* **B 366** (1991) 122.
- [78] V. A. Fateev and Al. B. Zamolodchikov, *Phys. Lett.* **B 271** (1991) 91.
- [79] F. Ravanini, R. Tateo and A. Valeriani, *Int. J. Mod. Phys.* **A 8** (1993) 1707-1728, arXiv:hep-th/9207040.
- [80] G. Delfino, G. Mussardo and P. Simonetti, *Phys. Rev.* **D 51** (1995) 6620-6624, arXiv:hep-th/9410117.
- [81] P. Dorey, G. Siviour and G. Takács, *JHEP* **1503** (2015) 054, arXiv:1412.8442 [hep-th].
- [82] D. X. Horváth, P.E. Dorey and G. Takacs, *JHEP* **1607** (2016) 051, arXiv:1604.05635 [hep-th].
- [83] Al. B. Zamolodchikov, *J. Phys.* **A 39** (2006) 12847-12862.

- [84] M. J. Martins, *Phys. Rev. Lett.* **69** (1992) 2461-2464, arXiv:hep-th/9205024.
- [85] P. E. Dorey and F. Ravanini, *Int. J. Mod. Phys. A* **8** (1993) 873-894, arXiv:hep-th/9206052.
- [86] M.J. Martins, *Phys. Lett. B* **304** (1993) 111-114.
- [87] P. Dorey and F. Ravanini, *Nucl. Phys. B* **406** (1993) 708, arXiv:hep-th/9211115.
- [88] A. B. Zamolodchikov, *JETP Lett.* **43** (1986) 730–732.
- [89] Al. Zamolodchikov, *Nucl. Phys. B* **342** (1990) 695–720.
- [90] D.-L. Vu and T. Yoshimura, *SciPost Phys.* **6** (2019) 023, arXiv:1809.03197 [cond-mat.stat-mech].
- [91] B. Bertini, L. Piroli and Pasquale Calabrese, *Phys. Rev. Lett.* **120** (2018)176801, arXiv:1709.10096 [cond-mat.stat-mech].
- [92] O. Castro-Alvaredo, Y. Chen, B. Doyon and M. Hoogeveen, *J. Stat. Mech.* **1403** (2014) 03011, arXiv:1310.4779 [hep-th].
- [93] B. Doyon, *Nucl. Phys. B* **892** (2015) 190-210, arXiv:1410.0292 [cond-mat.str-el].
- [94] D. A. Kastor, E. J. Martinec and S. H. Shenker, *Nucl. Phys. B* **316** (1989), 590.
- [95] A. B. Zamolodchikov, *Fractional Spin Integrals of Motion in Perturbed Conformal Field Theory in the Proceedings Conference Beijing 1989, "Fields, strings and quantum gravity"*, 349.
- [96] R. Landauer, *IBM Journal of Research and Development* **1** (1957) 223–231.
- [97] M. Büttiker, *Phys. Rev. Lett.* **57** (1986)1761.
- [98] M. Büttiker, *Phys. Rev. B* **38** (1988) 9375.
- [99] R. Landauer, *Phys. Scr.* **1992** 110.
- [100] Al. B. Zamolodchikov, *Phys. Lett. B* **335** (1994) 436–443.
- [101] C. Destri and H. J. de Vega, *Phys. Rev. Lett.* **69** (1992) 2313–2317.
- [102] C. Destri and H. J. de Vega, *Nucl. Phys. B* **438** (1995) 413–454, arXiv:hep-th/9407117.
- [103] P. Dorey, C. Dunning and R. Tateo, *Nucl. Phys. B* **578** (2000) 699-727, arXiv:hep-th/0001185.
- [104] G. Feverati, F. Ravanini and G. Takács, *Phys. Lett. B* **430** (1998) 264-273, hep-th/9803104.
- [105] G. Feverati, F. Ravanini and G. Takács, *Phys. Lett. B* **444** (1998) 442-450, hep-th/9807160.
- [106] G. Feverati, F. Ravanini and G. Takács, *Nucl. Phys. B* **540** (1999) 543-586, hep-th/9805117.
- [107] G. Feverati, F. Ravanini and G. Takács, *Nucl. Phys. B* **570** (2000) 615-643, hep-th/9909031.
- [108] V. A. Fateev and A. B. Zamolodchikov, *Nucl. Phys. B* **280** (1987) 644-660.
- [109] M. J. Martins, *Phys. Lett. B* **277** (1992) 301-305, arXiv:hep-th/9201032.

A Low temperature expansion of the GHD equations for the A_2 flow

In the following we briefly review the main steps of deriving the low temperature behaviour of the A_2 model via the low temperature expansion of the GHD equations (2.5), (2.6), (2.8)

and (2.10). Considering first the RM and LM pseudo-energies in thermal states they are determined by

$$\begin{aligned}\varepsilon_{RM} &= \frac{M}{2T} e^\vartheta - \frac{1}{2\pi} \int d\vartheta' \frac{1}{\cosh(\vartheta - \vartheta')} \ln \left(1 + e^{\varepsilon_{LM}(\vartheta')} \right) \\ \varepsilon_{LM} &= \frac{M}{2T} e^{-\vartheta} - \frac{1}{2\pi} \int d\vartheta' \frac{1}{\cosh(\vartheta - \vartheta')} \ln \left(1 + e^{\varepsilon_{LM}(\vartheta')} \right),\end{aligned}\tag{A.1}$$

which are the rewriting of eqs. (3.1) and (3.3). In the lowest order in T , the pseudo-energies $\varepsilon_{RM}^{(0)}$ and $\varepsilon_{LM}^{(0)}$ equal the driving terms in (A.1) and the convolutions are neglected. The next order contributions are obtained by iterating (A.1) with $\varepsilon_{RM}^{(0)}$ and $\varepsilon_{LM}^{(0)}$ using expansion of the logarithmic expression in the rewriting of eq. (A.1)

$$\begin{aligned}\varepsilon_{RM}^{(1)} &= \frac{M}{2T} e^\vartheta - \frac{1}{2\pi} \int d\tilde{\vartheta} \frac{1}{\cosh \tilde{\vartheta}} \ln \left(1 + \exp \left[\left(\frac{M}{2T} e^{-\vartheta} \right) e^{-\tilde{\vartheta}} \right] \right) \\ \varepsilon_{LM}^{(1)} &= \frac{M}{2T} e^{-\vartheta} - \frac{1}{2\pi} \int d\tilde{\vartheta} \frac{1}{\cosh \tilde{\vartheta}} \ln \left(1 + \exp \left[\left(\frac{M}{2T} e^\vartheta \right) e^{\tilde{\vartheta}} \right] \right),\end{aligned}\tag{A.2}$$

which gives

$$\begin{aligned}\varepsilon_{RM}^{(1)} &= \frac{M}{2T} e^\vartheta - \frac{1}{2\pi} \left(\frac{\pi^2}{6} \frac{2T}{M} e^\vartheta - \frac{49\pi^4}{1260} \left(\frac{2T}{M} e^\vartheta \right)^3 + \dots \right) \\ \varepsilon_{LM}^{(1)} &= \frac{M}{2T} e^{-\vartheta} - \frac{1}{2\pi} \left(\frac{\pi^2}{6} \frac{2T}{M} e^{-\vartheta} - \frac{49\pi^4}{1260} \left(\frac{2T}{M} e^{-\vartheta} \right)^3 + \dots \right).\end{aligned}\tag{A.3}$$

$$\tag{A.4}$$

The leading order corrections for the pseudo-energies are hence

$$\begin{aligned}\varepsilon_{RM}^{(1)} &= \frac{M}{2T} e^\vartheta \left(1 - \frac{\pi}{3} \left(\frac{T}{M} \right)^2 + \mathcal{O}(T^4) \right) \\ &= \frac{M}{2\tilde{T}} e^\vartheta + \mathcal{O}(T^3) \\ \varepsilon_{LM}^{(1)} &= \frac{M}{2T} e^{-\vartheta} \left(1 - \frac{\pi}{3} \left(\frac{T}{M} \right)^2 + \mathcal{O}(T^4) \right) \\ &= \frac{M}{2\tilde{T}} e^{-\vartheta} + \mathcal{O}(T^3),\end{aligned}\tag{A.5}$$

where to simplify the formulas \tilde{T} was introduced as

$$\tilde{T} = T \left(1 + \frac{\pi}{3} \left(\frac{T}{M} \right)^2 \right).\tag{A.6}$$

We need to determine the minimal and maximal values of the RM and LM effective velocities in pure thermal states. The effective velocities are defined in eq. (2.7) and for their extremal values it is first necessary to calculate $(e'_j(\vartheta))^{\text{dr}}$ and $(p'_j(\vartheta))^{\text{dr}}$ in the limits $\vartheta \rightarrow \mp\infty$ for RM and LM particles respectively. For this goal we assume that in these limits the following Ansatz is valid

$$\begin{aligned} (e'_{RM}(\vartheta))^{\text{dr}} &\approx c'_{RM} e^\vartheta \\ (p'_{RM}(\vartheta))^{\text{dr}} &\approx c'^{p'}_{RM} e^\vartheta \\ (e'_{LM}(\vartheta))^{\text{dr}} &\approx -c'_{LM} e^{-\vartheta} \\ (p'_{LM}(\vartheta))^{\text{dr}} &\approx c'^{p'}_{LM} e^{-\vartheta}. \end{aligned} \tag{A.7}$$

Then the unknown coefficients are determined by the dressing equation (2.5), which read for $(e'(\vartheta))^{\text{dr}}$ as

$$\begin{aligned} c'_{RM} e^\vartheta &= \frac{M}{2} e^\vartheta - \frac{1}{2\pi} \int d\vartheta' \frac{1}{\cosh(\vartheta - \vartheta')} n_{LM}^{(1)}(\vartheta') c'_{LM} e^{-\vartheta'} \\ -c'_{LM} e^{-\vartheta} &= -\frac{M}{2} e^{-\vartheta} + \frac{1}{2\pi} \int d\vartheta' \frac{1}{\cosh(\vartheta - \vartheta')} n_{RM}^{(1)}(\vartheta') c'_{RM} e^{\vartheta'}. \end{aligned} \tag{A.8}$$

eq. (A.7) is indeed a consistent approximation of $(e'_j(\vartheta))^{\text{dr}}$ and $(p'_j(\vartheta))^{\text{dr}}$ in the limits $\vartheta \rightarrow \mp\infty$ for RM and LM particles. In the first line of eq. (A.8) the region where (A.7) is not valid for $(e'_{LM}(\vartheta))^{\text{dr}}$ is suppressed by $n_{LM}^{(1)}(\vartheta')$ in a super-exponential way. Expanding $\frac{1}{\cosh(\vartheta - \vartheta')}$ in eq. (A.8) and performing the integration, the following equations are obtained for (A.7):

$$\begin{aligned} c'_{RM} e^\vartheta &= \frac{M}{2} e^\vartheta - \frac{\pi}{12} c'_{LM} e^\vartheta \left(\frac{2\tilde{T}}{M} \right)^2 + \mathcal{O}(T^4 e^{3\vartheta}) \\ c'_{LM} e^{-\vartheta} &= \frac{M}{2} e^{-\vartheta} - \frac{\pi}{12} c'_{RM} e^{-\vartheta} \left(\frac{2\tilde{T}}{M} \right)^2 + \mathcal{O}(T^4 e^{3\vartheta}) \end{aligned} \tag{A.9}$$

and after similar manipulations for $(p'_j(\vartheta))^{\text{dr}}$

$$\begin{aligned} c'^{p'}_{RM} e^\vartheta &= \frac{M}{2} e^\vartheta + \frac{\pi}{12} c'^{p'}_{LM} e^\vartheta \left(\frac{2\tilde{T}}{M} \right)^2 + \mathcal{O}(T^4 e^{3\vartheta}) \\ c'^{p'}_{LM} e^{-\vartheta} &= \frac{M}{2} e^{-\vartheta} + \frac{\pi}{12} c'^{p'}_{RM} e^{-\vartheta} \left(\frac{2\tilde{T}}{M} \right)^2 + \mathcal{O}(T^4 e^{3\vartheta}), \end{aligned} \tag{A.10}$$

from which the coefficients in eq. (A.7) can be uniquely determined:

$$\begin{aligned}
c_{RM}^{e'} = c_{LM}^{e'} &= \frac{M}{2} \frac{1 - \frac{\pi}{3} \left(\frac{\tilde{T}}{M} \right)^2}{1 - \left(\frac{\pi}{3} \left(\frac{\tilde{T}}{M} \right)^2 \right)^2} + \mathcal{O}(T^4) \\
c_{RM}^{p'} = c_{LM}^{p'} &= \frac{M}{2} \frac{1 + \frac{\pi}{3} \left(\frac{\tilde{T}}{M} \right)^2}{1 - \left(\frac{\pi}{3} \left(\frac{\tilde{T}}{M} \right)^2 \right)^2} + \mathcal{O}(T^4)
\end{aligned} \tag{A.11}$$

which are correct up to the second order in T , that is $\tilde{T} \rightarrow T$ and from the denominators only T^2 terms are to keep. The minimal and maximal values for the RM and LM effective velocities are hence

$$\begin{aligned}
v_{RM}^{min} &= \frac{1 - \frac{\pi}{3} \left(\frac{T}{M} \right)^2}{1 - \frac{\pi}{3} \left(\frac{T}{M} \right)^2} + \mathcal{O}(T^4) \\
&= 1 - \frac{2\pi}{3} \left(\frac{T}{M} \right)^2 + \mathcal{O}(T^4) \\
v_{LM}^{max} &= -\frac{1 - \frac{\pi}{3} \left(\frac{T}{M} \right)^2}{1 - \frac{\pi}{3} \left(\frac{T}{M} \right)^2} + \mathcal{O}(T^4) \\
&= -\left(1 - \frac{2\pi}{3} \left(\frac{T}{M} \right)^2 \right) + \mathcal{O}(T^4).
\end{aligned} \tag{A.12}$$

It is easy to apply the above calculation for the partitioning protocol we are primarily interested in. At low temperatures v_{RM}^{min} and v_{LM}^{max} are the endpoints of the interval of ξ where the density profiles are constant where $n_{RM}(\vartheta, \xi) = n_{RM}^{(l)}(\vartheta)$ and $n_{LM}(\vartheta, \xi) = n_{LM}^{(r)}(\vartheta)$. As a consequence, the temperature T in (A.12) has to be modified; for the RM particles $T^{(r)}$ and for the LM particles $T^{(l)}$ has to be used leading to

$$\begin{aligned}
c_{RM}^{e'} &= \frac{M}{2} \frac{1 - \frac{\pi}{3} \left(\frac{\tilde{T}_r}{M} \right)^2}{1 - \left(\frac{\pi}{3} \left(\frac{\tilde{T}_r}{M} \right)^2 \right) \left(\frac{\pi}{3} \left(\frac{\tilde{T}_l}{M} \right)^2 \right)} + \mathcal{O}(T^4) \\
c_{RM}^{p'} &= \frac{M}{2} \frac{1 + \frac{\pi}{3} \left(\frac{\tilde{T}_r}{M} \right)^2}{1 - \left(\frac{\pi}{3} \left(\frac{\tilde{T}_r}{M} \right)^2 \right) \left(\frac{\pi}{3} \left(\frac{\tilde{T}_l}{M} \right)^2 \right)} + \mathcal{O}(T^4) \\
c_{LM}^{e'} &= \frac{M}{2} \frac{1 - \frac{\pi}{3} \left(\frac{\tilde{T}_l}{M} \right)^2}{1 - \left(\frac{\pi}{3} \left(\frac{\tilde{T}_r}{M} \right)^2 \right) \left(\frac{\pi}{3} \left(\frac{\tilde{T}_l}{M} \right)^2 \right)} + \mathcal{O}(T^4) \\
c_{LM}^{p'} &= \frac{M}{2} \frac{1 + \frac{\pi}{3} \left(\frac{\tilde{T}_l}{M} \right)^2}{1 - \left(\frac{\pi}{3} \left(\frac{\tilde{T}_r}{M} \right)^2 \right) \left(\frac{\pi}{3} \left(\frac{\tilde{T}_l}{M} \right)^2 \right)} + \mathcal{O}(T^4)
\end{aligned} \tag{A.13}$$

which are correct only up to 2nd order in the temperature and hence the velocity bounds read

$$\begin{aligned}
v_{RM}^{min} &= 1 - \frac{2\pi}{3} \left(\frac{T_r}{M} \right)^2 + \mathcal{O}(T^4) \\
v_{LM}^{max} &= - \left(1 - \frac{2\pi}{3} \left(\frac{T_l}{M} \right)^2 \right) + \mathcal{O}(T^4),
\end{aligned} \tag{A.14}$$

which equal [72].

Thanks to the known expressions (A.13) for $(e'_j(\vartheta))^{\text{dr}}$ and $(p'_j(\vartheta))^{\text{dr}}$ we can easily calculate the energy and momentum densities and currents when $\xi \in [v_{LM}^{max}, v_{RM}^{min}]$ using the second lines in eqs. (2.6) and (2.8). The corresponding formulas, which are correct up to 4th order in the temperature, are as follows:

$$\begin{aligned}
q_e &= \frac{\pi}{24} \left[\frac{M}{2} c_{RM}^{p'} \left(\frac{2\tilde{T}_l}{M} \right)^2 + \frac{M}{2} c_{LM}^{p'} \left(\frac{2\tilde{T}_r}{M} \right)^2 \right] + \mathcal{O}(T^6) \\
j_e &= \frac{\pi}{24} \left[\frac{M}{2} c_{RM}^{e'} \left(\frac{2\tilde{T}_l}{M} \right)^2 - \frac{M}{2} c_{LM}^{e'} \left(\frac{2\tilde{T}_r}{M} \right)^2 \right] + \mathcal{O}(T^6) \\
q_p &= \frac{\pi}{24} \left[\frac{M}{2} c_{RM}^{p'} \left(\frac{2\tilde{T}_l}{M} \right)^2 - \frac{M}{2} c_{LM}^{p'} \left(\frac{2\tilde{T}_r}{M} \right)^2 \right] + \mathcal{O}(T^6) \\
j_p &= \frac{\pi}{24} \left[\frac{M}{2} c_{RM}^{e'} \left(\frac{2\tilde{T}_l}{M} \right)^2 + \frac{M}{2} c_{LM}^{e'} \left(\frac{2\tilde{T}_r}{M} \right)^2 \right] + \mathcal{O}(T^6),
\end{aligned} \tag{A.15}$$

which we can rewrite as

$$\begin{aligned}
q_e &= \frac{\pi}{24} \left[T_l^2 + T_r^2 + \frac{2\pi M^2}{3} \left\{ \left(\frac{T_l}{M} \right)^4 + \left(\frac{T_l}{M} \right)^2 \left(\frac{T_r}{M} \right)^2 + \left(\frac{T_r}{M} \right)^4 \right\} \right] + \mathcal{O}(T^6) \\
j_e &= \frac{\pi}{24} \left[T_l^2 \left(1 + \frac{2\pi}{3} \left(\frac{T_l}{M} \right)^2 \right) - T_r^2 \left(1 + \frac{2\pi}{3} \left(\frac{T_r}{M} \right)^2 \right) \right] + \mathcal{O}(T^6) \\
q_p &= \frac{\pi}{24} \left[T_l^2 \left(1 + \frac{2\pi}{3} \left(\frac{T_l}{M} \right)^2 \right) - T_r^2 \left(1 + \frac{2\pi}{3} \left(\frac{T_r}{M} \right)^2 \right) \right] + \mathcal{O}(T^6) \\
j_p &= \frac{\pi}{24} \left[T_l^2 + T_r^2 + \frac{2\pi M^2}{3} \left\{ \left(\frac{T_l}{M} \right)^4 - \left(\frac{T_l}{M} \right)^2 \left(\frac{T_r}{M} \right)^2 + \left(\frac{T_r}{M} \right)^4 \right\} \right] + \mathcal{O}(T^6).
\end{aligned} \tag{A.16}$$

B Hydrodynamics of the $W_5^3 \rightarrow W_4^3$ massless model

The W_p^3 models [108] are CFTs with an extended symmetry algebra, whose generators are spin-3 currents. These models possess a \mathbb{Z}_3 symmetry and can be regarded as certain generalisations of the critical 3-states Potts model, which is recovered for $p = 4$. The central charge is given by

$$c = 2 \left(1 - \frac{12}{p(p+1)} \right), \tag{B.1}$$

with $p \geq 4$. A particular perturbation of these models by the field Φ_3 with $\Delta = 1 - \frac{3}{p+1}$ results in integrable massless flows from W_p^3 to W_{p-1}^3 .

A TBA description for the W_p^3 massless flows (and also for massive perturbations) was proposed in [109] which are related to the A_2 Dynkin diagram in a non-trivial way. For the particular case of the $W_5^3 \rightarrow W_4^3$ flow the TBA equations contain only RM and LM species but each species is doubled. The corresponding TBA system reads

$$\begin{aligned}
\varepsilon_{RM}^a(\vartheta) &= \frac{M}{2T} e^\vartheta - \left(K_{ab} \star \ln \left(1 + e^{-\varepsilon_{RM}^b} \right) \right) (\vartheta) \\
&\quad + \left(K_{ab} \star \ln \left(1 + e^{-\varepsilon_{LM}^b} \right) \right) (\vartheta) \\
\varepsilon_{LM}^a(\vartheta) &= \frac{M}{2T} e^{-\vartheta} - \left(K_{ab} \star \ln \left(1 + e^{-\varepsilon_{LM}^b} \right) \right) (\vartheta) \\
&\quad + \left(K_{ab} \star \ln \left(1 + e^{-\varepsilon_{RM}^b} \right) \right) (\vartheta),
\end{aligned} \tag{B.2}$$

where $a, b = 1, 2$ and with the kernels

$$\begin{aligned}
K_{11}(\vartheta) &= K_{22}(\vartheta) = -\frac{\sqrt{3}}{2 \cosh \vartheta - 1} \\
K_{12}(\vartheta) &= K_{21}(\vartheta) = -\frac{\sqrt{3}}{2 \cosh \vartheta + 1}.
\end{aligned} \tag{B.3}$$

The one-particle energies and momentum are

$$\begin{aligned} e_{RM/LM}^{1,2} &= \frac{M}{2} e^{\pm\vartheta} \\ p_{RM/LM}^{1,2} &= \mp \frac{M}{2} e^{\pm\vartheta}. \end{aligned} \quad (\text{B.4})$$

The Euler scale hydrodynamics of this model is easy to obtain. Figure 7 shows the profiles for various left and right temperatures and table 5 displays the values of the effective and dynamical central charges. These are in accordance with our previous findings, such as the broad plateaux in the profiles, the bound on the dynamical central charges and the monotonicity of \tilde{c}_{j_e} . Moreover, regions of constant densities and currents appear in the profiles for low temperatures as a consequence of the lack of magnonic particles in the TBA system.

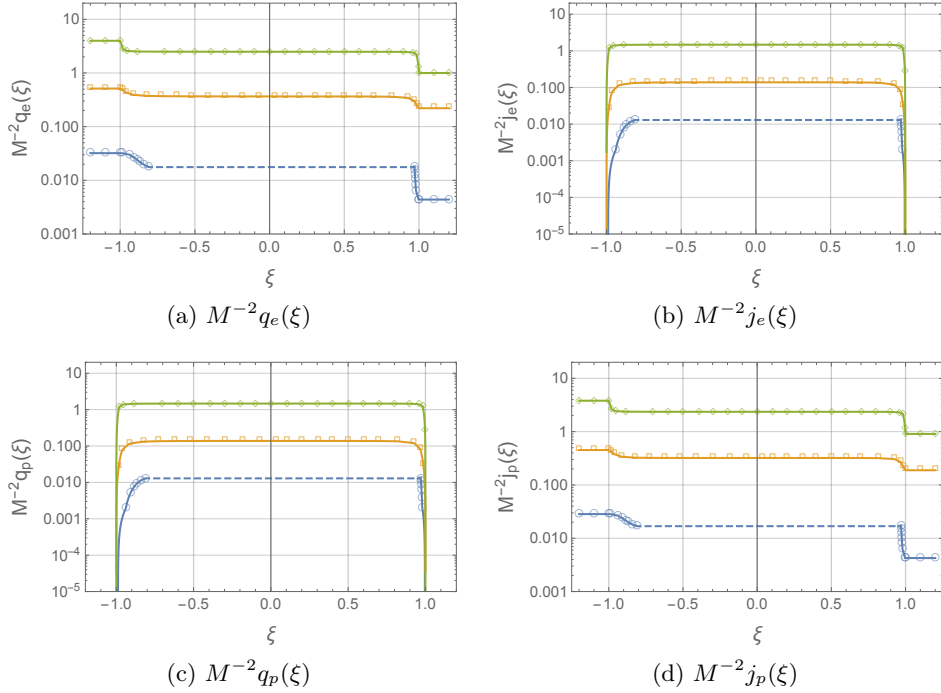


Figure 7: Ray-dependent (a) energy density q_e , (b) energy current j_e , (c) momentum density q_p and (d) momentum current j_p in the $W_5^3 \rightarrow W_4^3$ massless flow after bipartite quenches at the Euler scale. The green curve with diamonds corresponds to left and right initial temperatures $T_l = 2.5M$ and $T_r = 1.25M$, the orange curve with squares to $T_l = 0.9M$ and $T_r = 0.6M$ and the blue curve with circles to $T_l = 0.25M$ and $T_r = 0.1M$. The discrete points in the plots indicated by the plotmarkers are obtained by the numerical solution of GHD equations, the continuous curves are first order interpolations. The dashed part of the curves indicates the region of constant densities and currents. Due to relativistic invariance, $j_e = q_p$.

T_l/M	T_r/M	$\tilde{c}(T_l)$	$\tilde{c}(T_r)$	$\tilde{c}_{j_e}(T_l, T_r)$	$\tilde{c}_{q_e}(T_l, T_r)$	$\tilde{c}_{j_p}(T_l, T_r)$	$\tilde{c}_{j_e}^{lb}(T_l, T_r)$
0.25	0.1	0.868088	0.811868	0.93966	0.928449	0.88748	0.878801
0.6	0.3	1.0011	0.890578	1.1193	1.12183	0.991055	1.03793
0.9	0.6	1.06489	1.0011	1.17196	1.19334	1.047	1.11592
0.9	0.85	1.06489	1.05658	1.1807	1.20618	1.06099	1.1335
0.95	0.9	1.07249	1.06489	1.18307	1.20934	1.06891	1.13906
1.1	0.1	1.09176	0.811868	1.14362	1.16375	1.12339	1.09408
1.4	0.9	1.11894	1.06489	1.18975	1.21554	1.10385	1.157
2.5	1.25	1.16275	1.10687	1.19694	1.21587	1.15202	1.18136
5.5	5.0	1.18864	1.18681	1.19973	1.20689	1.18777	1.19729
6	0.6	1.19009	1.0011	1.19854	1.20418	1.18918	1.19196
6	5	1.19009	1.18681	1.19974	1.20642	1.18871	1.19751
9	8.5	1.19482	1.19432	1.19976	1.2033	1.19453	1.19888

Table 5: The effective central charges for (left and right) thermal states and the dynamical central charges for the partitioning protocol for various left and right temperatures in the $W_5^3 \rightarrow W_4^3$ massless flow, where $c_{UV} = 1.2$ and $c_{IR} = 0.8$.